

<sup>1</sup> The effects of drought on land cover change and vegetation productivity in  
<sup>2</sup> continental Chile

<sup>3</sup> Francisco Zambrano<sup>a,b,\*</sup>, Anton Vrieling<sup>c</sup>, Francisco Meza<sup>d,e,f</sup>, Iongel Duran-Llacer<sup>g</sup>, Francisco Fernández<sup>h,i</sup>,  
<sup>4</sup> Alejandro Venegas-González<sup>j</sup>, Nicolas Raab<sup>d</sup>, Dylan Craven<sup>l,1</sup>

<sup>a</sup>Hémera Centro de Observación de la Tierra, Facultad de Ciencias, Escuela de Ingeniería en Medio Ambiente y Sustentabilidad, Universidad Mayor, Santiago, 7500994, Chile.

<sup>b</sup>Observatorio de Sequía para la Agricultura y la Biodiversidad de Chile (ODES), Universidad Mayor, Santiago, 7500994, Chile.

<sup>c</sup>Faculty of Geo-Information Science and Earth, University of Twente, Enschede, The Netherlands.

<sup>d</sup>Facultad de Agronomía y Sistemas Naturales, Pontificia Universidad Católica de Chile., Santiago, Chile.

<sup>e</sup>Instituto para el Desarrollo Sustentable. Pontificia Universidad Católica de Chile, Santiago, Chile.

<sup>f</sup>Centro Interdisciplinario de Cambio Global, Pontificia Universidad Católica de Chile, Santiago, Chile.

<sup>g</sup>Hémera Centro de Observación de la Tierra, Facultad de Ciencias, Universidad Mayor,, Santiago, 7500994, Chile.

<sup>h</sup>Center of Economics for Sustainable Development (CEDES), Faculty of Economics and Government, Universidad San Sebastián, Santiago, Chile.

<sup>i</sup>Center of Applied Ecology and Sustainability (CAPES), Santiago, Chile.

<sup>j</sup>Instituto de Ciencias Agroalimentarias, Animales y Ambientales (ICA3), Universidad de O'Higgins, San Fernando, Chile.

<sup>k</sup>, GEMA Center for Genomics, Ecology & Environment, Universidad Mayor, Camino La Pirámide Huechuraba 5750, Santiago, Chile.

<sup>l</sup>Data Observatory Foundation, Santiago, Chile.

---

<sup>5</sup> **Abstract**

Chile has experienced a persistent decrease in water supply, which impacts the hydrological system and vegetation development. This persistent period of water scarcity has been defined as a mega-drought. There is yet insufficient understanding of ecological drought in Chile due to the limited studies on the relationship between drought and ecosystem changes. The aim of our study is to evaluate the interaction of drought, land cover change, and vegetation productivity over continental Chile. To assess drought, we used drought indices for atmospheric evaporative demand (AED), water supply, and soil moisture from short- (1, 3, 6 months) to long-term (12, 24, 36 months) time scales. We derived the drought indices using monthly ERA5-Land reanalysis data from 1981 to 2023. We used Moderate-Resolution Imaging Spectroradiometer (MODIS) datasets to derive information on annual land cover and monthly vegetation productivity. Our results showed that, except for the Austral part, Chile has a temporal decreasing trend in water supply, and across the whole country, there is an increase in AED. These trends become stronger over longer time scales. We found a negative trend in vegetation productivity in the north-central area, which is more prominent for shrubland and savanna as compared to croplands and forests. The anomaly in soil moisture over the past 12 months (SSI-12) is the most important variable explaining these changes, followed by anomalies in accumulated precipitation over one to two years (SPI-12 and SPI-24). The variable importance obtained by random forest models indicates that drought explains about 12–41% of the change in land cover surface across Chile for forest, grassland, shrubland, and savanna but has little relation to the changes in croplands. The increase in AED is the main variable associated with the change in land cover, followed by a reduction in precipitation and soil moisture. Our findings provide insightful information that could assist in developing adaptation measures for Chilean ecosystems to cope with climate change and drought.

6 *Keywords:* drought, land cover change, vegetation productivity, ecosystem

---

7 **1. Introduction**

8 Drought can be classified as 1) meteorological, when precipitation in a specific period remains below the  
9 mean precipitation experienced in the same period during multiple years (more than 30 years usually); 2)  
10 hydrological, when these anomalies last for long periods (months to years) and affect water systems; and 3)  
11 agricultural, when the deficit negatively impacts plant health and leads to decreased productivity of crops  
12 or pastures (Wilhite and Glantz, 1985). However, because drought is also influenced by human activities,  
13 Van Loon et al. (2016) and AghaKouchak et al. (2021) expanded the drought definition for the Anthropocene,  
14 indicating that the feedback of human decisions and activities should also be considered (i.e., anthropogenic  
15 drought). Droughts can lead to increased tree mortality (Cheng et al., 2024) and induce alterations in land  
16 cover and land use, ultimately affecting ecosystems (Crausbay et al., 2017). Even though many ecological  
17 studies have at times mistakenly considered “dry” conditions as “drought” (Slette et al., 2019), ecological  
18 drought can be defined as “*an episodic deficit in water availability that drives ecosystems beyond thresholds of  
vulnerability, impacts ecosystem services, and triggers feedback in natural and/or human systems*” (Crausbay  
19 et al., 2017). In light of current global warming, it is crucial to study the interaction between drought and  
20 ecosystems in order to understand their feedback and impact on future water security (Bakker, 2012).

22 Global warming, as a result of human-induced greenhouse gas emissions, has increased the frequency and  
23 intensity of drought, according to the sixth assessment report (AR6) of the Intergovernmental Panel on  
24 Climate Change (IPCC) (Calvin et al., 2023). The evidence supporting this claim has been strengthened  
25 since AR5 (IPCC, 2013). Recent studies, however, have produced contrasting findings, with some suggesting  
26 that drought has not exhibited a significant trend over the past forty years (Vicente-Serrano et al., 2022;  
27 Kogan et al., 2020). Vicente-Serrano et al. (2022) analyzed the trend in meteorological drought on a global  
28 scale, finding that only in a few regions an increase in the severity of drought was observed. Moreover,  
29 they attributed this increase solely to an increase in atmospheric evaporative demand (AED) due to higher  
30 temperatures, which in turn enhances vegetation water demand, with important implications for agricultural  
31 and ecological droughts. Also, they state that “*the increase in hydrological droughts has been primarily  
observed in regions with high water demand and land cover change, led by an increase in agricultural land*”.  
32 Similarly, Kogan et al. (2020) analyzed the drought trend using remotely-sensed vegetation health indicators,  
33 finding that for the globe and main grain-producing countries, drought has not expanded or intensified during  
34 the past 38 years. Nonetheless, Masson-Delmotte (2021) suggests that there is a medium to high degree  
35 of confidence that rising temperatures will increase the extent, frequency, and severity of agricultural and  
36 ecological droughts. Also, AR6 (Calvin et al., 2023) predicts that many regions of the world will experience  
37 more severe agricultural and ecological droughts even if global warming stabilizes at 1.5°–2°C. To better  
38 evaluate the impact of drought trends on ecosystems, assessments of the relationship between meteorological  
39 and soil moisture variables and their effects on vegetation are much needed.

41 From 1960 to 2019, land use change has impacted around one-third of the Earth’s surface, which is four  
42 times more than previously thought (Winkler et al., 2021). Multiple studies aim to analyze and forecast  
43 changes in land cover globally (Winkler et al., 2021; Song et al., 2018) and regionally (Chamling and Bera,  
44 2020; Homer et al., 2020; Yang and Huang, 2021; Schulz et al., 2010; Echeverría et al., 2012). Some seek  
45 to analyze the impact of land cover change on climate conditions such as temperature and precipitation  
46 (Luyssaert et al., 2014; Pitman et al., 2012). There is less research on drought and its relation to land cover  
47 change and vegetation productivity (Chen et al., 2022; Akinyemi, 2021; Peng et al., 2017). Peng et al. (2017)  
48 utilized net primary productivity to examine the spatial and temporal variations in vegetation productivity  
49 at global level and assess to what extent drought influenced this variability by comparing the twelve-month

---

\*Corresponding author

Email addresses: francisco.zambrano@umayor.cl (Francisco Zambrano), a.vrieling@utwente.nl (Anton Vrieling)

50 Standardized Precipitation Evapotranspiration Index (SPEI) and land cover change. According to their  
51 findings, drought is responsible for 37% of the decline and accounts for 55% of the variability in vegetation  
52 productivity. [Chen et al. \(2022\)](#) instead found poor correlations ( $r<0.2$ ) between the vegetation productivity  
53 trends against meteorological drought (SPEI of twelve months in December) and soil moisture at the global  
54 level. These studies mostly looked at how changes in land cover and vegetation productivity are related to a  
55 single drought index (SPEI) obtained for 12 month periods. SPEI takes into account the combined effect of  
56 precipitation and AED as a water balance, but it does not allow to know the contribution of each variable on  
57 its own. To better understand these contributions on land cover change and vegetation productivity the  
58 following questions may be asked: i) how do land cover and vegetation productivity respond to short- to  
59 long-term meteorological and soil moisture droughts? And ii) how is this response different between humid  
60 and arid climatic zones? Likewise, there is a lack of understanding of how the alteration in water supply and  
61 demand is affecting land cover transformations.

62 To address the previous questions over extensive regions, we can utilize gridded data on water availability,  
63 vegetation conditions, and the respective drought indices. For monitoring drought, the World Meteorological  
64 Organization recommends the SPI (Standardized Precipitation Index) ([WMO et al., 2012](#)). The SPI is a  
65 multi-scalar drought index that only uses precipitation to assess short- to long-term droughts. [Vicente-Serrano  
66 et al. \(2010\)](#) proposed the Standardized Precipitation Evapotranspiration Index (SPEI), which incorporates  
67 the temperature effect by subtracting AED from precipitation. SPEI allows for analyzing the combined effect  
68 of precipitation and AED. Since its formulation, it has been used worldwide for the study and monitoring  
69 of drought ([Gebrechorkos et al., 2023; Liu et al., 2024](#)). Recently, there has been more interest in using  
70 AED to track droughts separately to better disentangle precipitation from temperature-dependent effects  
71 ([Vicente-Serrano et al., 2020](#)). One of the reasons is that AED is more linked to flash droughts in water-limited  
72 regions ([Noguera et al., 2022](#)). [Hobbins et al. \(2016\)](#) and [McEvoy et al. \(2016\)](#) developed the Evaporative  
73 Demand Drought Index (EDDI) to monitor droughts solely using the AED, and it has proven effective in  
74 monitoring flash droughts ([Li et al., 2024; Ford et al., 2023](#)). For soil moisture, several drought indices  
75 exist, such as the Soil Moisture Deficit Index (SDMI) ([Narasimhan and Srinivasan, 2005](#)) and the Soil  
76 Moisture Agricultural Drought Index (SMADI) ([Souza et al., 2021](#)). [Hao and AghaKouchak \(2013\)](#) and  
77 [AghaKouchak \(2014\)](#) proposed the Standardized Soil Moisture Index (SSI), which has a similar formulation  
78 as the SPI, SPEI, and EDDI. Thus, many drought indices exist that allow for a comprehensive assessment  
79 of drought on short- to long-term scales and that allow for the use of single variables from Earth's water  
80 balance (e.g., precipitation, AED, soil moisture). Climatic variability impacts vegetation development, with  
81 unfavorable conditions such as low precipitation and high temperatures usually promoting a decrease in plant  
82 productivity. To monitor the response of vegetation for large areas, the common practice is to use satellite  
83 data. For example, the Normalized Difference Vegetation Index (NDVI) derived from frequent satellite  
84 observations of red and near infrared spectral reflectance, has been widely used as a proxy for biomass  
85 production [Camps-Valls et al. \(2021\); Paruelo et al. \(2016\); Helman et al. \(2014\)](#). For Chile's cultivated  
86 land, [Zambrano et al. \(2018\)](#) used the zcNDVI for assessing seasonal biomass production in response to  
87 drought. Comparing the various meteo-related and vegetation-based drought indices, we can further our  
88 understanding of the impact of drought on ecosystems.

89 Chile's diverse climatic and ecosystem types ([Beck et al., 2023; Luebert and Pliscoff, 2022](#)) make it an ideal  
90 natural laboratory for studying climate and ecosystems. Additionally, the country has experienced severe  
91 drought conditions that have had significant effects on vegetation and water storage. North-central Chile has  
92 faced a persistent precipitation deficit since 2010, defined as a mega-drought ([Garreaud et al., 2017](#)), which  
93 has impacted the Chilean ecosystem and consequently makes it highly vulnerable to climate change ([Barría  
94 et al., 2021; Alvarez-Garreton et al., 2021](#)). This mega-drought was defined by the annual time series of the  
95 Standardized Precipitation Index (SPI) at a time scale of twelve months at the end of each year (December)  
96 when having values below one standard deviation. Some studies have addressed how this drought affects  
97 single ecosystems in terms of forest growth ([Miranda et al., 2020; Venegas-González et al., 2018](#)), forest fire  
98 occurrence ([Urrutia-Jalabert et al., 2018](#)), and crop productivity ([Zambrano, 2023b; Zambrano et al., 2018,  
99 Zambrano et al. \(2016\)](#)). The term "mega-drought" is used in Chile to describe a prolonged water shortage  
100 that lasts for several years, resulting in a permanent deficit that impacts the hydrological system ([Boisier](#)

101 et al., 2018). Therefore, it is crucial to evaluate temporal scales that consider the cumulative impact over  
102 a period of several years. In Chile, the relationship between drought and the environment remains poorly  
103 understood. Hence, we aim to contribute to understanding how climatic and soil moisture droughts influence  
104 ecosystem dynamics in order to provide useful information that helps for a better understanding of ecological  
105 droughts and, at the same time, helps to make well-informed decisions on adaptation strategies.

106 Here, we analyze the multi-dimensional impacts of drought across ecosystems in continental Chile. More  
107 specifically, we aim to assess: i) short- to long-term temporal trends in multi-scalar drought indices; ii)  
108 temporal changes in land-use cover and the direction and magnitude of their relationships with trends in  
109 drought indices; and iii) the trend in vegetation productivity and its relationship with drought indices across  
110 Chilean ecosystems.

## 111 2. Study area

112 Continental Chile has diverse climate conditions with strong gradients from north to south and east to  
113 west (Aceituno et al., 2021) Figure 1a, which determines its great ecosystem diversity (Luebert and Pliscoff,  
114 2022) (Figure 1c). The Andes Mountains are a main factor in climate variation (Garreaud, 2009). For  
115 an aggregated overview of the results of the study, we used the five Chilean macrozones: “Norte Grande”  
116 (17°34'–25°42'S), “Norte Chico” (25°42'–32°8'S), “Centro” (32°08'–36°12'S), “Sur” (36°12'–43°48'S), and  
117 “Austral” (43°48'–56°00'S). “Norte Grande” and “Norte Chico” predominate in an arid desert climate with  
118 hot (Bwh) and cold (Bwk) temperatures. At the south of “Norte Chico”, the climate changes to an arid  
119 steppe with cold temperatures (Bsk). In these two northern regions, the land is mostly bare, with a small  
120 surface of vegetation types such as shrubland and grassland. In the macrozones “Centro” and the northern  
121 half of “Sur”, the main climate is Mediterranean, with warm to hot summers (Csa and Csb). Land cover in  
122 “Centro” comprises a significant amount of shrubland and savanna (50%), grassland (16%), forest (8%), and  
123 croplands (5%). An oceanic climate (Cfb) predominates in the south of “Sur” and the north of “Austral”.  
124 Those zones have a large area of forest and grassland. The southern part of the country has a tundra climate,  
125 while “Austral” is a cold semi-arid area with an extended surface of grassland, forest, and, to a lesser extent,  
126 savanna.

## 127 3. Materials and Methods

### 128 3.1. Data

#### 129 3.1.1. Gridded meteorological and vegetation data

130 To analyze land cover change, we used the classification scheme by the IGBP (International Geosphere-  
131 Biosphere Programme) from the product MCD12Q1 Collection 6.1 from MODIS. The MCD12Q1 product  
132 is produced for each year from 2001 to 2022 and defines 17 classes (see Table S1). To maintain our focus  
133 on a large scale and follow the FAO classification (FAO, 2022), we considered native and planted forests as  
134 “forests”, which represent ecosystems dominated by larger trees. To derive a proxy for vegetation productivity,  
135 we used the Normalized Difference Vegetation Index (NDVI) from the product MOD13A3 Collection 6.1  
136 from MODIS (Didan, 2015). MOD13A3 provides vegetation indices with 1km spatial resolution and monthly  
137 frequency. The NASA EOSDIS Land Processes Distributed Active Archive Center (LP DAAC), USGS Earth  
138 Resources Observation and Science (EROS) Center, Sioux Falls, South Dakota, provided the MOD13A3 and  
139 MCD12Q1 from the online Data Pool, accessible at <https://lpdaa.usgs.gov/tools/data-pool/>.

140 For soil moisture, water supply, and water demand variables, we used ERA5-Land (ERA5L) (ECMWF  
141 Reanalysis version 5 over land) (Muñoz-Sabater et al., 2021), a reanalysis dataset that provides the evolution  
142 of atmospheric and land variables since 1950. It has a spatial resolution of 0.1° (9 km), hourly frequency,  
143 and global coverage. We selected the variables for total precipitation, maximum and minimum temperature  
144 at 2 meters, and volumetric soil water layers between 0 and 100 cm of depth (layer 1 to layer 3). Table 1  
145 shows a summary of the data and its main characteristics.

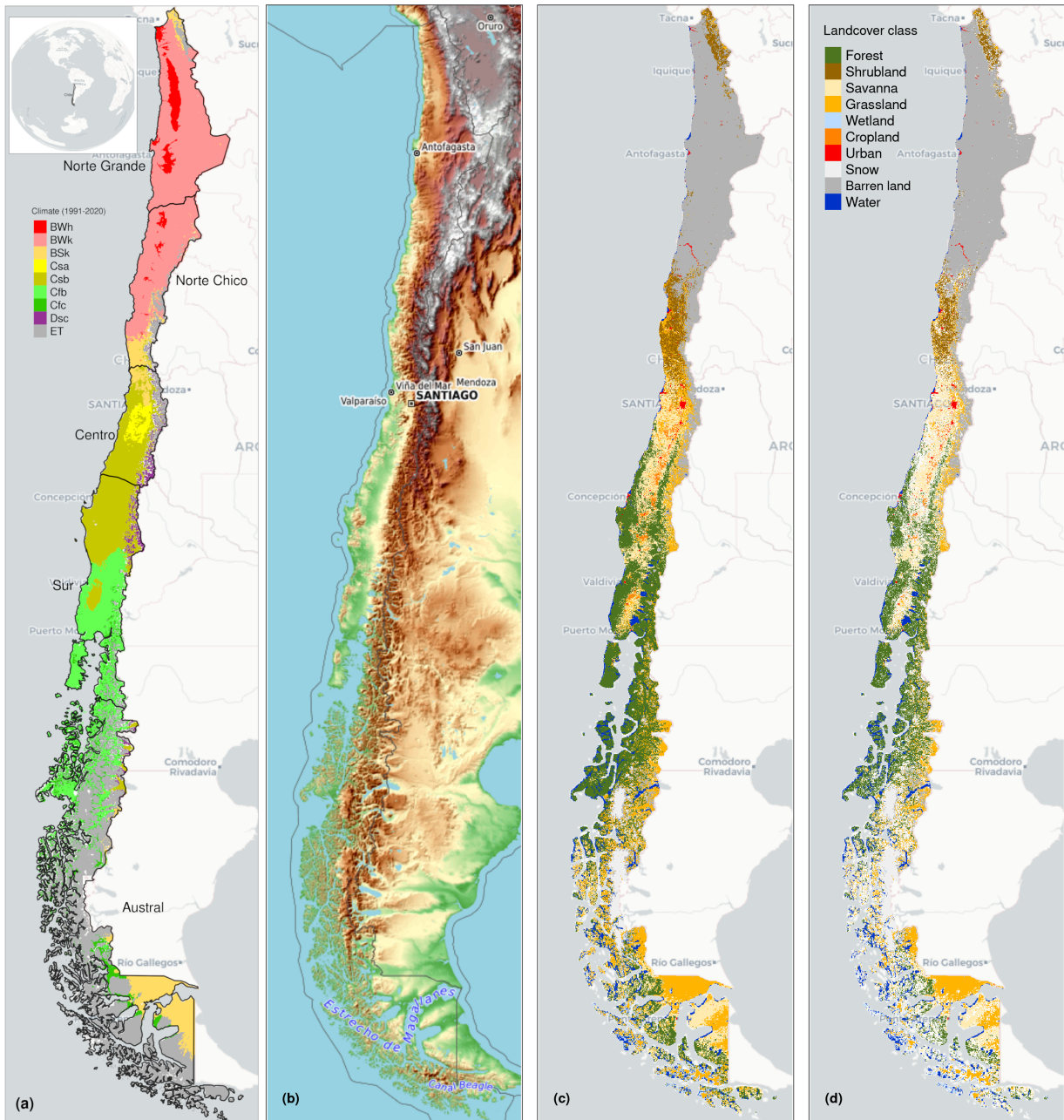


Figure 1: (a) Chile with the Koppen-Geiger climate classes and the five macrozones “Norte Grande”, “Norte Chico”, “Centro”, “Sur”, and “Austral”. (b) Topography reference map. (c) land cover classes for 2022. (d) Persistent land cover classes (> 80% for 2001-2022)

146    3.2. Short- to long-term drought trends

147    3.2.1. Atmospheric Evaporative Demand (AED)

148    To compute the drought indices that use water demand, it is necessary to first calculate the AED. To do  
 149    this, we employed the Hargreaves method (Hargreaves, 1994; Hargreaves and Samani, 1985) by applying the  
 150    following equation:

| Product | Sub-product | Variable                               | [!ht] | Spatial Resolution | Period    | Units | Short Name |
|---------|-------------|--|-------|--------------------|-----------|-------|------------|
| ERA5L   |             | Precipitation                          |       |                    |           | mm    | P          |
|         |             | Maximum temperature                    |       | 0.1°               | 1981-2023 | °C    | $T_{max}$  |
|         |             | Minimum temperature                    |       |                    |           | °C    | $T_{min}$  |
| ERA5L*  |             | Volumetric Soil Water Content at 1m    |       |                    |           | m³/m³ | SM         |
|         |             | Atmospheric Evaporative Demand         |       | 0.1°               | 1981-2023 | mm    | AED        |
| MODIS   | MOD13A3.061 | Normalized Difference Vegetation Index |       | 1 km               | 2000-2023 |       | NDVI       |
|         | MCD12Q1.061 | land cover IGBP scheme                 |       |                    | 2001-2022 |       | land cover |

\*Calculated from maximum and minimum temperatures derived from ERA5L with Eq. 1.

Table 1: Description of the satellite and reanalysis data used

$$AED = 0.0023 \cdot Ra \cdot (T + 17.8) \cdot (T_{max} - T_{min})^{0.5} \quad (1)$$

where  $Ra$  ( $MJ m^2 day^{-1}$ ) is extraterrestrial radiation;  $T$ ,  $T_{max}$ , and  $T_{min}$  are mean, maximum, and minimum temperature ( $^{\circ}C$ ) at 2m. For calculating  $Ra$  we used the coordinate of the latitud of the centroid of each pixel as follow:

$$Ra = \frac{14,400}{\pi} \cdot G_{sc} \cdot d_r [\omega_s \cdot \sin(\phi) \cdot \sin(\delta) + \cos(\phi) \cdot \cos(\delta) \cdot \sin(\omega_s)] \quad (2)$$

where:

$Ra$ : extraterrestrial radiation [ $MJ m^{-2} day^{-1}$ ],

$G_{sc}$ : solar constant = 0.0820 [ $MJ m^{-2} min^{-1}$ ],

$d_r$ : inverse relative distance Earth-Sun,

$\omega_s$ : sunset hour angle [rad],

$\phi$ : latitude [rad],

$\delta$ : solar declination [rad].

We chose the method of Hargreaves to estimate AED because of its simplicity, which only requires temperatures and extrarrestrial radiation. Also, it has been recommended over other methods (e.g., Penman-Monteith) when the access to climatic variables is limited (Vicente-Serrano et al., 2014).

### 3.2.2. Non-parametric calculation of drought indices

To derive the drought indices of water supply and demand, soil moisture, and vegetation (i.e., the proxy of productivity), we used the ERA5L dataset and the MODIS product, with a monthly frequency for 1981–2023 and 2000–2023, respectively. The drought indices correspond to a historical anomaly of a variable (e.g., meteorological, vegetation, or soil moisture). To account for the anomaly, the common practice is to derive it following a statistical parametric method in which it is assumed that the statistical distribution of the data is known (Heim, 2002). The use of an erroneous statistical distribution that does not fit the data is usually the highest source of uncertainty (Laimighofer and Laaha, 2022). In the case of Chile, due to its high degree of climatic variability, it is difficult to choose a proper distribution without previous research that could be applicable throughout Chile. Here, we follow a non-parametric method for the calculation of the drought indices, in a similar manner as the framework proposed by Farahmand and AghaKouchak (2015).

For the purpose of monitoring water supply drought, we used the well-known Standardized Precipitation Index (SPI), which relies on precipitation data. To evaluate water demand, we chose the Evaporative Demand Drought Index (EDDI), developed by Hobbins et al. (2016) and McEvoy et al. (2016), which is based on the AED. The United States currently monitors drought using the EDDI (<https://psl.noaa.gov/eddi/>) as an experimental index. To consider the combined effect of water supply and demand, we selected the SPEI (Vicente-Serrano et al., 2010). For SPEI, an auxiliary variable  $D = P - AED$  is calculated. Soil moisture is the main driver of vegetation productivity, particularly in semi-arid regions (Li et al., 2022). Hence, for soil

water drought, we used the SSI (Standardized Soil Moisture Index) (Hao and AghaKouchak, 2013). For the SSI, we used the average soil moisture from ERA5L at 1m depth. Finally, for the proxy of productivity, we used the zcNDVI (Zambrano et al., 2018), which was derived from the monthly time series of NDVI derived from MOD13A1. All the indices are multi-scalar and can be used for the analysis of short- to long-term droughts.

To derive the drought indices, we first calculate the sum of the variables with regard to the time scale(s). In this case, for generalization purposes, we will use  $V$ , referring to variables  $P$ ,  $AED$ ,  $D$ ,  $NDVI$ , and  $SM$  (Table 1). We accumulated each over the time series of values (months), and for the time scales  $s$ :

$$A_i^s = \sum_{i=n-s-i+2}^{n-i+1} V_i \quad \forall i \geq n - s + 1 \quad (3)$$

The  $A_i^s$  corresponds to a moving window (convolution) that sums the variable for time scales  $s$ . This summation is done over  $s$  months, starting from the most recent month ( $n$ ) back in time until month  $n - s + 1$ . For example, using as a variable the precipitation, a period of twelve months ( $n$ ), and a time scale of three months ( $s$ ), it will be:

$$\begin{aligned} A_1^3 &= P_{oct} + P_{nov} + P_{dic} \\ &\vdots = \vdots + \vdots + \vdots \\ A_{10}^3 &= P_{jan} + P_{feb} + P_{mar} \end{aligned}$$

Then, we used the empirical Tukey plotting position (Wilks, 2011) over  $A_i^s$  to derive the  $P(A_i^s)$  probabilities across a period of interest:

$$P(A_i^s) = \frac{i - 0.33}{n + 0.33} \quad (4)$$

An inverse normal approximation (Abramowitz and Stegun, 1968) obtains the empirically derived probabilities once the variable cumulates over time for the scale  $s$ . Thus, the drought indices  $SPI$ ,  $SPEI$ ,  $EDDI$ ,  $SSI$ , and  $zcNDVI$  and obtained following the equation:

$$DI(A_i^s) = W - \frac{C_0 + C_1 \cdot W + c_2 \cdot W^2}{1 + d_1 \cdot W + d_2 \cdot W^2 + d_3 \cdot W^3} \quad (5)$$

$DI$  is referring to the drought index calculated for the variable  $V$  (i.e., SPI, SPEI, EDDI, SSI, and zcNDVI). The values for the constats are:  $C_0 = 2.515517$ ,  $C_1 = 0.802853$ ,  $C_2 = 0.010328$ ,  $d_1 = 1.432788$ ,  $d_2 = 0.189269$ , and  $d_3 = 0.001308$ . For  $P(A_i^s) \leq 0.5$ ,  $W = \sqrt{-2 \cdot \ln(P(A_i^s))}$ , and for  $P(A_i^s) > 0.5$ , replace  $P(A_i^s)$  with  $1 - P(A_i^s)$  and reverse the sign of  $DI(A_i^s)$ .

The drought indices were calculated for time scales of 1, 3, 6, 12, 24, and 36 months at a monthly frequency for 1981–2023 in order to be used for short- to long-term evaluation of drought.

For the proxy of vegetation productivity, we chose the time scale that best correlates with annual net primary productivity (NPP) across continental Chile. For this purpose, we calculated the zcNDVI for time scales of 1, 3, 6, and 12 months in December and compared it with the annual NPP. We used the NPP from the MOD17A3HGF (Running and Zhao, 2019) dataset (MODIS). We chose to use six months because the  $R^2$  between zcNDVI and NPP reaches its highest value at six months. We obtained an  $R^2$  of 0.31 for forest and 0.72 for shrubland (refer to the supplementary material in Section S5). Then, we chose the proxy of vegetation productivity for six months, which we will name zcNDVI hereafter. It was calculated at a monthly frequency for 2000–2023.

213    3.2.3. *Trend of drought indices*

214    To estimate if there are significant positive or negative trends for the drought indices, we used the non-  
215 parametric Mann-Kendall test (Kendall, 1975). To determine the magnitude of the trend, we used Sen's slope  
216 (Sen, 1968). Sen's slope has the advantage over normal regression that it is less affected by outliers, and as a  
217 non-parametric method it is not influenced by the distribution of the data. We applied the Mann-Kendall  
218 test to see if the trend was significant and Sen's slope to estimate the magnitude of the trend. We did this  
219 for the indices SPI, EDDI, SPEI, and SSI using the six time scales with data from 1981 to 2023 (monthly  
220 frequency), resulting in 24 trends (per index and time scale). Then, we extracted the trend aggregated  
221 by each of the five macrozones: "Norte Grande" to "Austral", and per land cover type: grassland, forest,  
222 cropland, shrubland, savanna, and barren land (Figure 1d).

223    3.3. *Interaction of land cover and drought*

224    3.3.1. *Land cover change*

225    To analyze the land cover change, we use the IGBP scheme from the MCD12Q1 Collection 6.1 from MODIS.  
226 This product has been previously used for studies of drought and land cover in Chile (Fuentes et al., 2021;  
227 Zambrano et al., 2018). We regrouped the 17 classes into ten macroclasses, as follows: classes 1-4 to forest,  
228 5-7 to shrublands, 8-9 to savannas, 10 as grasslands, 11 as wetlands, 12 and 14 to croplands, 13 as urban, 15  
229 as snow and ice, 16 as barren, and 17 to water bodies (Table S1). Thus, we have a land cover raster time  
230 series with the ten macroclasses for 2001 and 2023. We validate the land cover macroclasses regarding a  
231 highly detailed (30 m of spatial resolution) land cover map made for Chile by Zhao et al. (2016) for 2013-2014.  
232 Our results showed a global accuracy of ~0.82 and a F1 score of ~0.66. Section S2 in the Supplementary  
233 Material shows the procedure for validation.

234    We calculated the surface occupied per land cover class into the five macrozones ("Norte Grande" to  
235 "Austral") per year for 2001–2022. After that, we calculated the trend's change in surface per land cover type  
236 and macroclass. We used Mann-Kendall for the significance of the trend (Kendall, 1975) and Sen's slope to  
237 calculate the magnitude (Sen, 1968).

238    To assess how water demand and supply, and soil moisture affect the variation in vegetation productivity  
239 across various land cover types, we avoid analyzing areas that experienced major land cover changes in the  
240 2021–2022 period. To assess how zcNDVI varied irrespective of land cover change, we developed a persistence  
241 mask for land cover, which only retains pixels for which the macroclass remained the same for at least 80%  
242 of the 22 years (Figure 1d).

243    3.3.2. *Relationship between land cover and drought trends*

244    To identify which drought indices and time scales have a major impact on changes in land cover type, we  
245 examined the relationship between the trend in land cover classes and the trend in drought indices. To have  
246 more representative results, we conducted the analysis over sub-basins within continental Chile. We used  
247 469 basins, which have a surface area between 0.0746 and 24,000 km<sup>2</sup> and a median area of 1,249 km<sup>2</sup>. For  
248 each basin, we calculated the trend per land cover type, considering the proportion of the type relative to  
249 the total surface of the basin. Then, we extracted per basin the average trend (Sen's slope) of the drought  
250 indices SPI, SPEI, EDDI, SSI, and all their time scales 1, 3, 6, 12, 24, and 36. Also, we extracted the average  
251 trend in the proxy of vegetation productivity (zcNDVI).

252    We model the trends in land cover per macroclass with the aim of assessing how land cover trends relate  
253 to drought indices. We used the random forest method (Ho, 1995), which employs multiple decision trees,  
254 allowing for classification and regression. Some advantages include the ability to find non-linear relationships,  
255 reduce overfitting, and derive variable importance. We included the four drought indices per six time scales  
256 and the zcNDVI, totaling 25 predictors. As a result, we created thirty random forest models, one for each  
257 land cover macroclass trend and per macrozone. Each model was trained using 1000 forests in a resampling  
258 scheme to obtain more reliable results regarding variable importance. We resampled by creating ten folds,  
259 running a random forest per fold, and calculating the R<sup>2</sup>, root mean square error (RMSE), and variable  
260 importance. The variable importance helps for a better understanding of the relationships by finding which

variable has a higher contribution to the model. Thus, we calculated the variable's importance by permuting out-of-bag (OOB) data per tree and computing the mean standard error in the OOB. After permuting each predictor variable, we repeated the process for the remaining variable. We repeated this process ten times (per fold) to obtain the performance metrics ( $R^2$ , RMSE, and variable importance).

Finally, we visually explored the connection between the SPI, EDDI, and SSI drought indices for short- and long-term changes in land cover. To do this, we compared the relative changes in land cover surface (in terms of the total surface area per land cover type and macrozone) with the drought indices of six (short-term) and thirty-six months (long-term).

### 3.4. Drought impacts on vegetation productivity

For each land cover macroclass, we analyzed the trend of vegetation productivity over the unchanged land cover macroclasses. To achieve this, we used the persistent mask of land cover macroclasses, thus reducing the possibility of evaluating productivity trends that are due to year-to-year variation in land cover. We used the zcNDVI as a proxy of vegetation productivity. To assess productivity in Chile's cultivated land, Zambrano et al. (2018) used the zcNDVI for assessing seasonal biomass production in relation to climate.

We examined the drought indices of water demand, water supply, and soil moisture and their correlation with vegetation productivity. The objective is to determine to what extent soil moisture and water demand and supply affect vegetation productivity, thus addressing three main questions: 1) Which of the drought variables—supply, demand, or soil moisture—helps most in explaining the changes in vegetation productivity? 2) How do the short- to long-term time scales of the drought variable affect vegetation productivity in Chile, and how strong is the relationship? And finally, 3) how does the correlation vary per-land cover type? Answering these questions should advance our understanding of how climate is affecting vegetation, considering the impact on the five land cover types: forest, cropland, grassland, savanna, and shrubland.

We conducted an analysis on the linear correlation between the indices SPI, SPEI, EDDI, and SSI over time periods of 1, 3, 6, 12, 24, and 36 months with zcNDVI. We used a method similar to that used by Meroni et al. (2017) which compared the SPI time-scales with the cumulative fAPAR (fraction of Absorbed Photosynthetically Active Radiation). We performed a pixel-to-pixel linear correlation analysis for each index within the persistent mask of land cover macroclasses. We first compute the Pearson coefficient of correlation for each of the six time scales. A time scale is identified as the one that attains the highest correlation ( $p < 0.05$ ). We then extracted the Pearson correlation coefficient corresponding to the time scales where the value peaked. As a result, for each index, we generated two raster maps: 1) containing the raster with values of the time scales and drought index that reached the maximum correlation, and 2) having the magnitude of the correlation obtained by the drought index at the time scales.

### 3.5. Software

For the downloading, processing, and analysis of the spatio-temporal data, we used the open source software for statistical computing and graphics, R (R Core Team, 2023). For downloading ERA5L, we used the {ecmwf} package (Hufkens et al., 2019). For processing raster data, we used {terra} (Hijmans, 2023) and {stars} (Pebesma and Bivand, 2023). For managing vectorial data, we used {sf} (Pebesma, 2018). For the calculation of AED, we used {SPEI} (Beguería and Vicente-Serrano, 2023). For mapping, we used {tmap} (Tennekes, 2018). For data analysis and visualization, the suite {tidyverse} (Wickham et al., 2019) was used. For the random forest modeling, we used the {tidymodels} (Kuhn and Wickham, 2020) and {ranger} (Wright and Ziegler, 2017) packages.

## 4. Results

### 4.1. Short- to long-term drought trends

Figure 2 shows the spatial variation of the trend for the drought indices from short- to long-term scales. SPI and SPEI have a decreasing trend from “Norte Chico” to “Sur”, but an increasing trend in “Austral”.

<sup>306</sup> The degree of the trend is larger at higher time scales. In “Norte Grande”, the SSI increased in the southwest  
<sup>307</sup> and decreased in the northeast, for all time scales. Similar to SPI and SPEI, SSI decreases at higher time  
<sup>308</sup> scales. EDDI showed a positive trend for the whole of continental Chile, with a higher slope toward the  
<sup>309</sup> north and a descending gradient toward the south. The slope of trend increases at higher time scales.

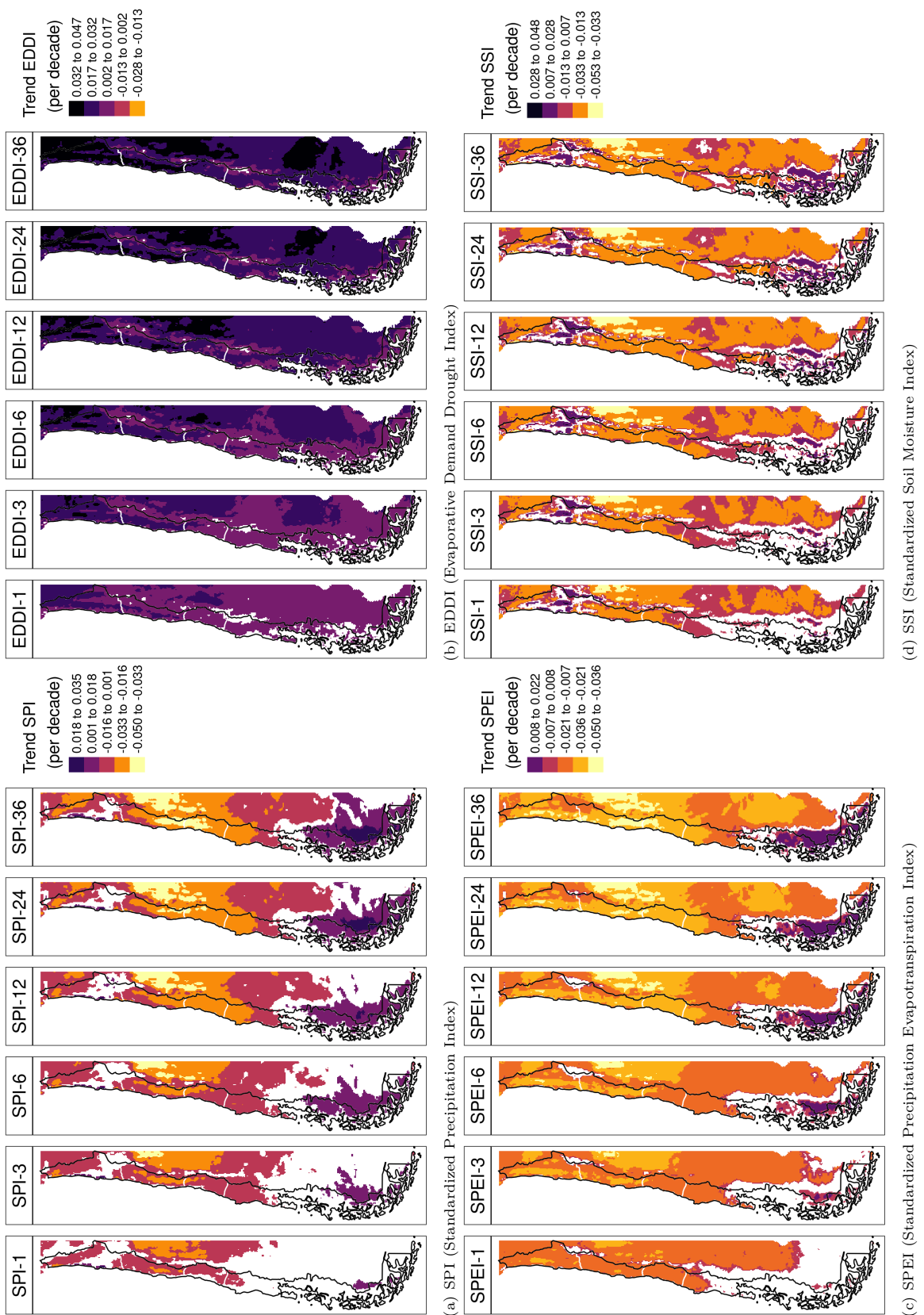


Figure 2: Linear trend of the drought index (\*) at time scales of 1, 3, 6, 12, 24, and 36 months for 1981-2023

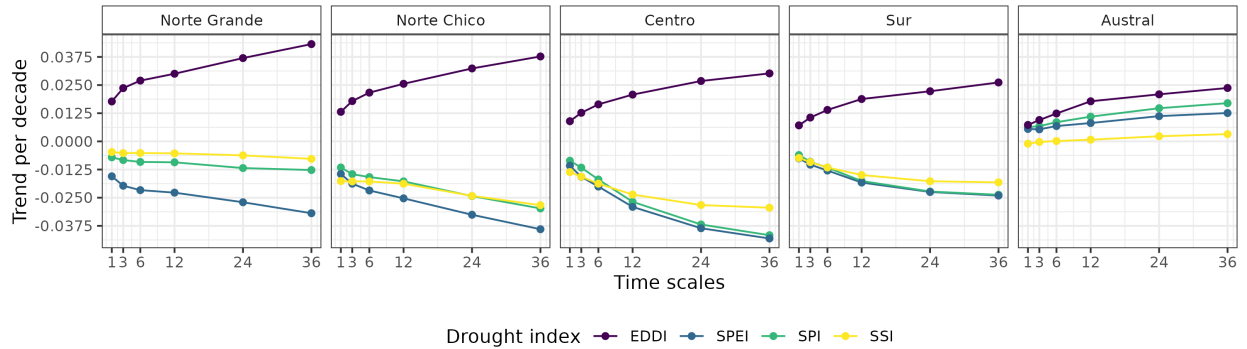


Figure 3: Trend per decade for the drought indices SPI, EDDI, SPEI, and SSI aggregated by macrozone.

310 The Figure 3 displays the aggregated trend per macrozone, drought index, and timescale. The macrozones  
 311 that reached the lowest trend for SPI, SPEI, and SSI are “Norte Chico” and “Centro”, where the indices also  
 312 decrease at longer time scales. This may potentially be explained by the prolonged reduction in precipitation  
 313 that has affected the hydrological system in Chile. At 36 months, it reaches trends between -0.03 and -0.04  
 314 (z-score) per decade for SPI, SPEI, and SSI. For “Sur”, the behavior is similar, decreasing at longer scales  
 315 and having between -0.016 and -0.025 per decade for SPI, SPEI, and SSI. “Norte Grande” has the highest  
 316 trend at 36 months for EDDI (0.042 per decade), and “Centro” has the lowest for SPI and SPEI. In “Norte  
 317 Grande” and “Norte Chico”, which are in a semi-arid climate, it is evident that the EDDI has an effect on  
 318 the difference between the SPI and SPEI index, which is not seen in the other macrozones. Contrary to the  
 319 other macrozones, “Austral” showed an increase in all indices, being the highest for EDDI at 36 months  
 320 (0.025) and the lowest for SSI, which shows only a minor increase in the trend.

#### 321 4.2. Interaction of land cover and drought

##### 322 4.2.1. Land cover change

Table 2: Surface per land cover class that persists during 2001–2022.

| Surface [km <sup>2</sup> ] |         |          |           |         |           |             |
|----------------------------|---------|----------|-----------|---------|-----------|-------------|
| Macrozone                  | Forest  | Cropland | Grassland | Savanna | Shrubland | Barren land |
| Norte Grande               |         |          | 886       |         | 7,910     | 171,720     |
| Norte Chico                |         | 90       | 4,283     | 589     | 16,321    | 84,274      |
| Centro                     | 3,739   | 1,904    | 7,584     | 19,705  | 844       | 12,484      |
| Sur                        | 72,995  | 1,151    | 7,198     | 15,906  |           | 2,175       |
| Austral                    | 60,351  |          | 54,297    | 19,007  | 249       | 7,218       |
| Total                      | 137,085 | 3,145    | 74,247    | 55,206  | 25,324    | 277,870     |

323 For vegetation, we obtained and used hereafter five macroclasses of land cover from IGBP MODIS: forest,  
 324 shrubland, savanna, grassland, and croplands. Figure 1c shows the spatial distribution of the macroclasses  
 325 through Chile for the year 2022. Figure 1d shows the macroclasses of land cover persistence (80%) during  
 326 2021–2022, respectively (Table 2). Within continental Chile, barren land is the land cover class with the  
 327 highest surface area ( $277,870 \text{ km}^2$ ). The largest type of vegetation, with  $137,085 \text{ km}^2$ , is forest. Grassland  
 328 has  $74,247 \text{ km}^2$ , savanna  $55,206 \text{ km}^2$ , shrubland  $25,341 \text{ km}^2$ , and cropland  $3,146 \text{ km}^2$  (Table 2). The  
 329 macrozones with major changes for 2001–2022 were “Centro”, “Sur”, and “Austral”, with 36%, 31%, and  
 330 34% of their surface changing the type of land cover, respectively (Figure 1 and Table 3). Figure 4 shows the  
 331 variation for 2001–2022 in the proportion of surface per land cover class and macrozone, derived from the  
 332 persistence mask over continental Chile.

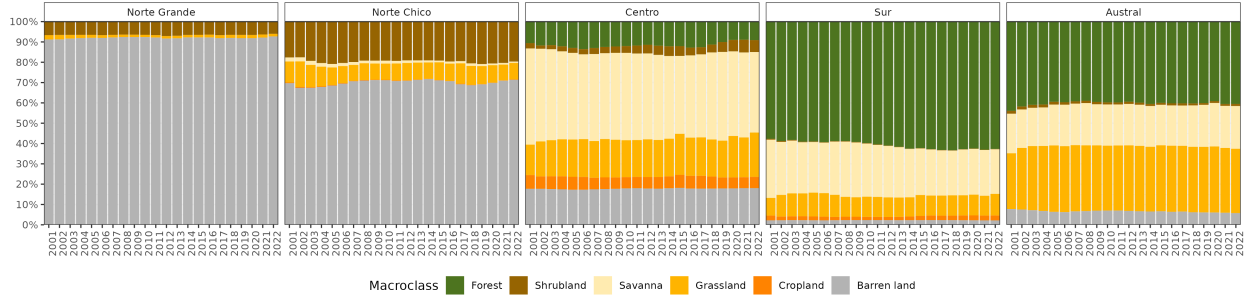
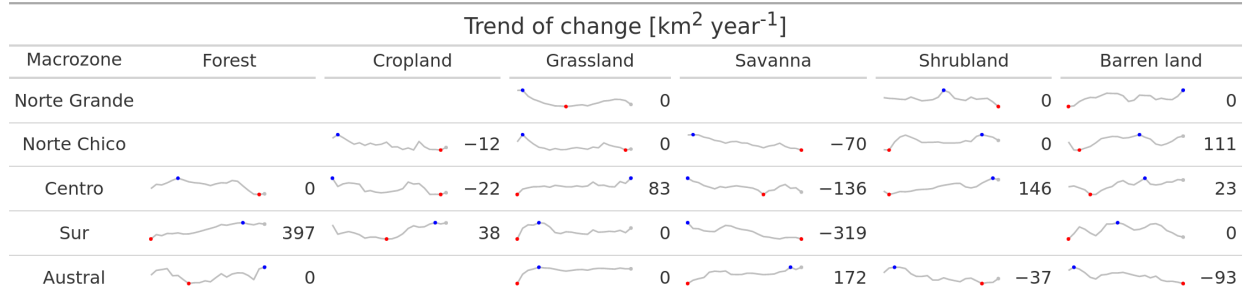


Figure 4: Proportion of land cover class from the persistent land cover for 2001–2022 (>80%) per macrozone and land cover macroclass.

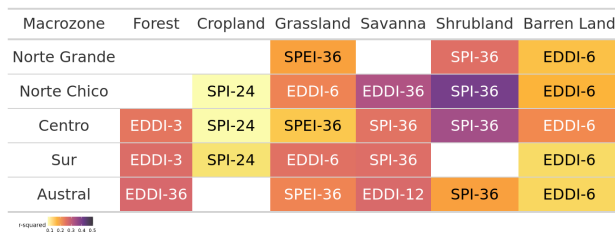
Table 3: The value of Sen's slope trend next to the time-series plot of surface per land cover class (IGBP MCD12Q1.016) for 2001–2022 through Central Chile. Values of zero indicate that there was not a significant trend. The red dots on the plots indicate the maximum and minimum values of the surface. The white cells indicate that the landcover class is not significant in terms of surface area.



333 From the trend analysis in Table 3, we can indicate that the “Norte Chico” shows an increase in barren  
 334 land of  $111 \text{ km}^2 \text{ yr}^{-1}$  and a reduction in the class savanna of  $70 \text{ km}^2 \text{ yr}^{-1}$ . In the “Centro” and “Sur”, there  
 335 are changes with an important reduction in savanna with  $136$  and  $319 \text{ km}^2 \text{ yr}^{-1}$ , respectively, and an increase  
 336 in shrubland and grassland, showing a change for more dense vegetation types. The area under cultivation  
 337 (croplands) appears to be shifting from the “Centro” to the “Sur”. Also, there is a high increase in forest  
 338 ( $397 \text{ km}^2 \text{ yr}^{-1}$ ) in the “Sur”, seemingly replacing the savanna lost (Table 3).

#### 339 4.2.2. Relationship between drought indices and land cover change

Table 4: The five most important trends of drought indices in estimating the landcover trend per land cover type and the  $R^2$  reached by each random forest model. The white cells indicate that the landcover class is not significant in terms of surface area.



340 Table 4 shows the drought indices that are the most important variables in the random forest models,  
 341 together with the  $R^2$  reached. The random forest models reached an  $R^2$  between 0.12 and 0.41 for the land  
 342 cover types and macrozones. The model shows the highest  $R^2$  for shrublands (0.28 to 0.42) and the lowest  
 343  $R^2$  for croplands (0.16 to 0.20) across all macrozones.

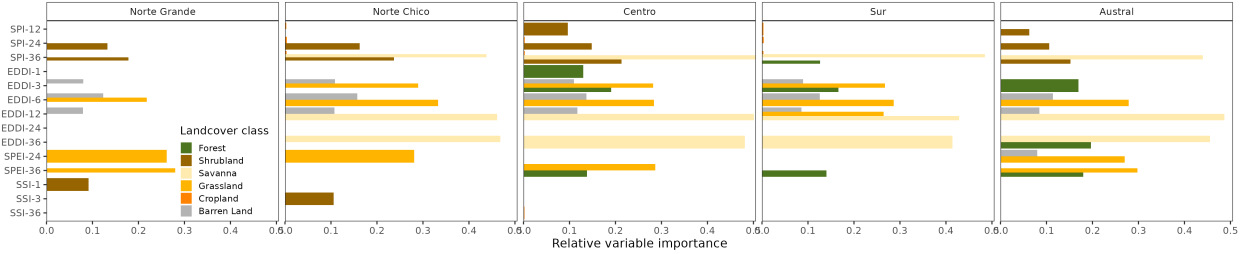


Figure 5: Relative importance of drought indices for explaining the trend in landcover change across the five macrozones in Chile. SPI, Standardized Precipitation Index; EDDI, Evaporative Demand Drought Index; SPEI, Standardized Precipitation Evapotranspiration Index; SSI, Standardized Soil Moisture Index. The numbers beside the drought index correspond to the time scales.

Figure 5 shows the three most important variables for the models across the five macrozones and per landcover type. For shrublands, the SPI of long-term and short-term SSI were the most relevant drought indices within the five macrozones. We showed that the trend in short-term EDDI (1–6 months) and long-term SPI (24- and 36-months) affected grasslands and forest changes. We showed that trends in SPI-36 and long-term trends in EDDI (12 to 36 months) were associated with changes in savannas. The changes in barren land are shown to be limited to the changes in the short-term AED (1 to 6 months). Changes in croplands have not been linked to drought across all macrozones. The supplementary material in Section S3 provides further details about the variable's importance.

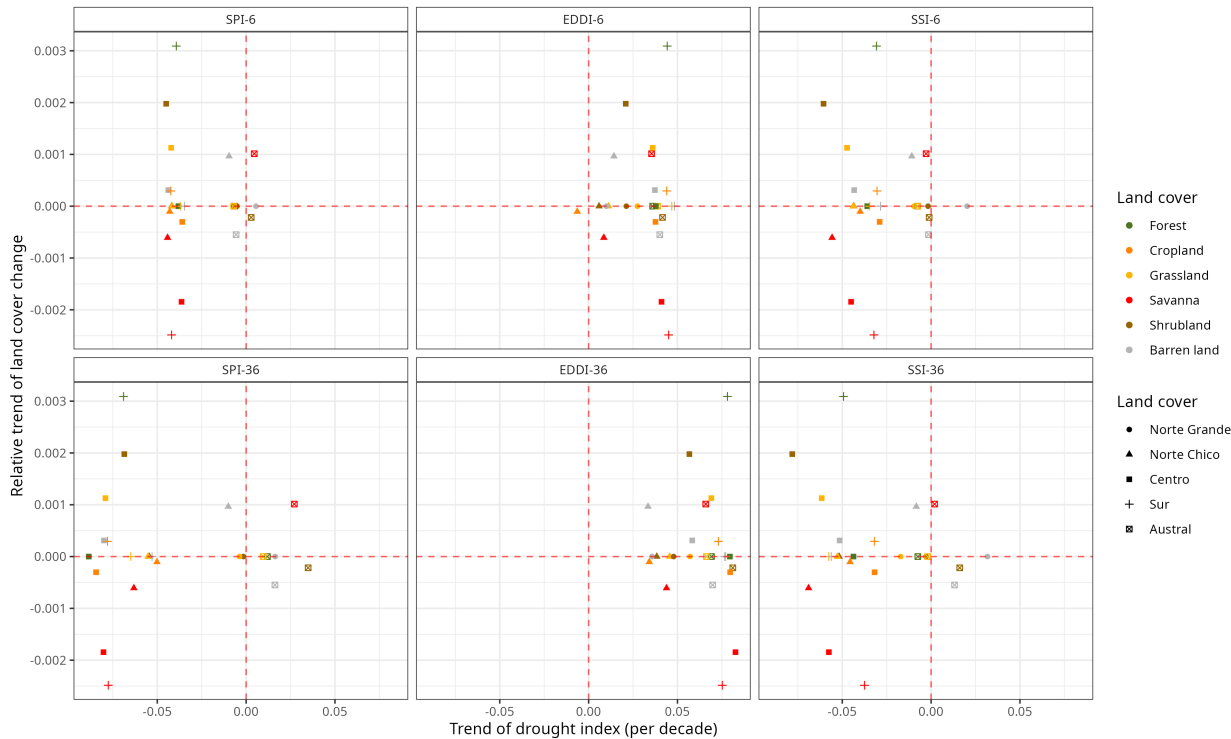


Figure 6: Relationship between the trend in land cover change (y-axis) and the trend in drought indices (x-axis) for the five macrozones. Vertical panels correspond to short (6 months) and long (36 months) time scales. Horizontal panels show the drought indices SPI, EDDI, and SSI.

Figure 6 shows the connection between the SPI, EDDI, and SSI drought indices for time scales of 6 and 36

months against changes in land cover. Forest in the “Sur”, shrubland and grassland in “Centro”, barren land in “Norte Chico”, and savanna in “Austral” showed an increase in land cover extent, which was associated with an increase in EDDI. Savanna in “Centro”, “Sur”, and “Norte Chico” decreases with the increase in EDDI. The SPI and SSI showed similar behavior regarding the trend in land cover type. A decrease in SPI and SSI is associated with an increase in the surface in shrubland and grassland in “Centro”, forest in “Sur”, and barren land in “Norte Chico”, as well as a decrease trend in savanna in “Norte Chico”, “Centro”, and “Sur”.

#### 4.3. Drought impacts on vegetation productivity within land cover

##### 4.3.1. Trends in vegetation productivity

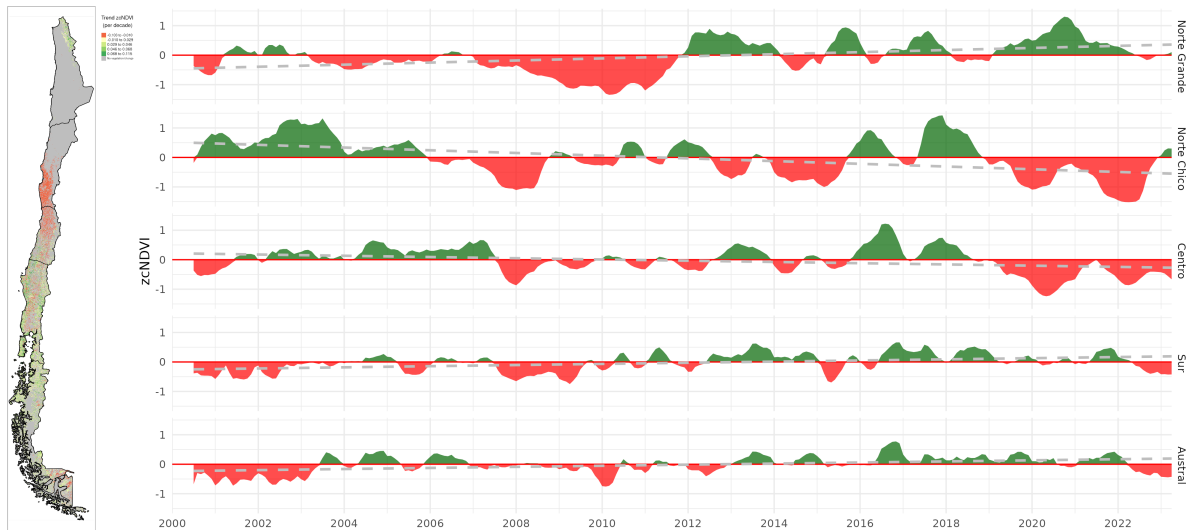


Figure 7: (a) Map of the linear trend of the index zcNDVI for 2000–2023. Greener colors indicate a positive trend; redder colors correspond to a negative trend and a decrease in vegetation productivity. Grey colors indicate either no vegetation or a change in land cover type for 2001–2022. (b) Temporal variation of zcNDVI aggregated at macrozone level within continental Chile. Each horizontal panel corresponds to a macrozone from ‘Norte Grande’ to ‘Austral’.

Figure 7 shows a spatial map of trends in zcNDVI (Figure 7a). In “Norte Grande”, vegetation productivity, as per the z-index, exhibits a yearly increase of 0.027 for grassland and 0.032 for shrubland. In “Norte Chico”, savanna has the lowest trend slope of -0.062, cropland -0.047, shrubland -0.042, and grassland -0.037. In “Centro”, shrubland reaches -0.07, savanna -0.031, cropland -0.024, forest -0.017, and grassland -0.005 per decade. This decrease in productivity could be associated either with a reduction in vegetation surface, a decrease in biomass, or browning.

The temporal variation within the macrozones is shown in Figure 7b. There is a negative trend in “Norte Chico” with -0.035 and “Centro” with -0.02 per decade. Vegetation reached its lowest values for 2019-2022, with an extreme condition in early 2020 and 2022 in the “Norte Chico” and “Centro”. The “Sur” and “Austral” show a positive trend of around 0.012 and 0.016, respectively, per decade (Figure 7).

##### 4.3.2. Correlation between vegetation productivity and drought indices

Figure 8 shows the time scales that reached the highest r-squared in the regression analysis between zcNDVI and different drought indicators over time scales of 1, 3, 6, 12, 24, and 36 months. The spatial variation of time scales reached per index is mostly for time scales above 12 months. In the case of SSI, the predominant scales are 6 and 12 months. For all indices, to the north, the time scales are higher and diminish toward the south until the south part of “Austral”, where they increase. In Figure 9, the map of Pearson correlation values ( $r$ ) is shown. The EDDI reached correlations above 0.5 between “Norte Chico” and “Sur”. The correlation changes from negative to positive toward the Andes Mountains and to the sea, just as in the

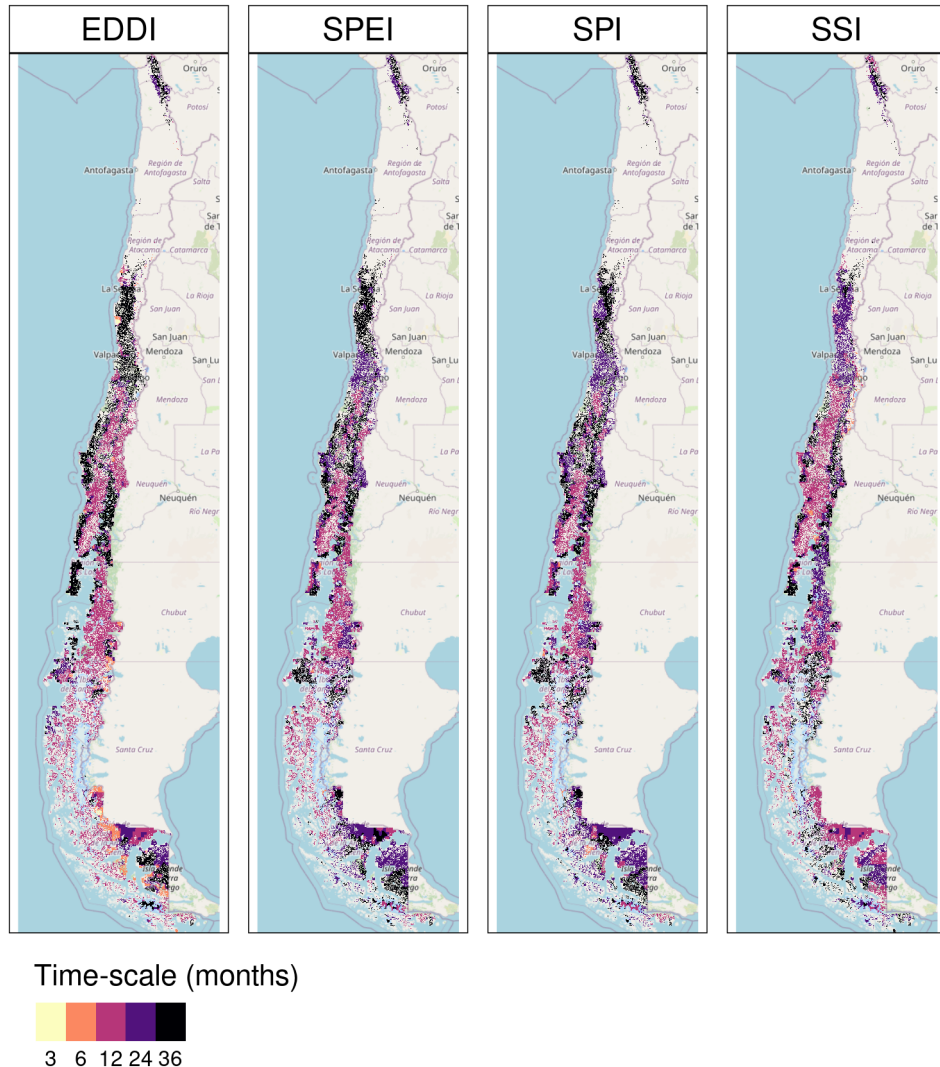


Figure 8: Time scales per drought index that reach the maximum coefficient of determination. White spaces indicate no significant correlation.

380 northern part of “Austral”. The SPI and SPEI have similar results, with the higher values in “Norte Chico”  
 381 and “Centro” being higher than 0.6. Following a similar spatial pattern as EDDI but with an opposite sign.  
 382 The SSI showed to be the index that has a major spatial extension with a higher correlation. It has a similar  
 383 correlation to SPI and SPEI for “Norte Chico” and “Centro”, but for “Sur” the correlation is higher with SSI.

384 In Table 5, we aggregate per macrozone and land cover the correlation analysis presented in Figure 8  
 385 and Figure 9. According to what is shown, forests is likely to be the most resistant to drought. Showing  
 386 that only “Centro” is slightly ( $R^2 = 0.25$ ) impacted by a 12-month soil moisture deficit (SSI-12).  
 387 In the “Norte Chico” and to a lesser extent in the “Norte Grande”, it is evident that a SSI-12 with  
 388 a  $R^2 = 0.45$  and a decrease in water supply (SPI-36 and SPEI-24 with  $R^2 = 0.28$  and 0.34, respec-  
 389 tively) have an impact on grasslands. However, this type was unaffected by soil moisture, water sup-  
 390 ply, or demand in macrozones further south. The types that show to be most affected by variation  
 391 in climate conditions are shrublands, savannas, and croplands. For savannas in “Norte Chico”, the  
 392 SSI-12 and SPI-24 reached an  $R^2$  of 0.74 and 0.58, respectively. This value decreases to the south, but the SSI –

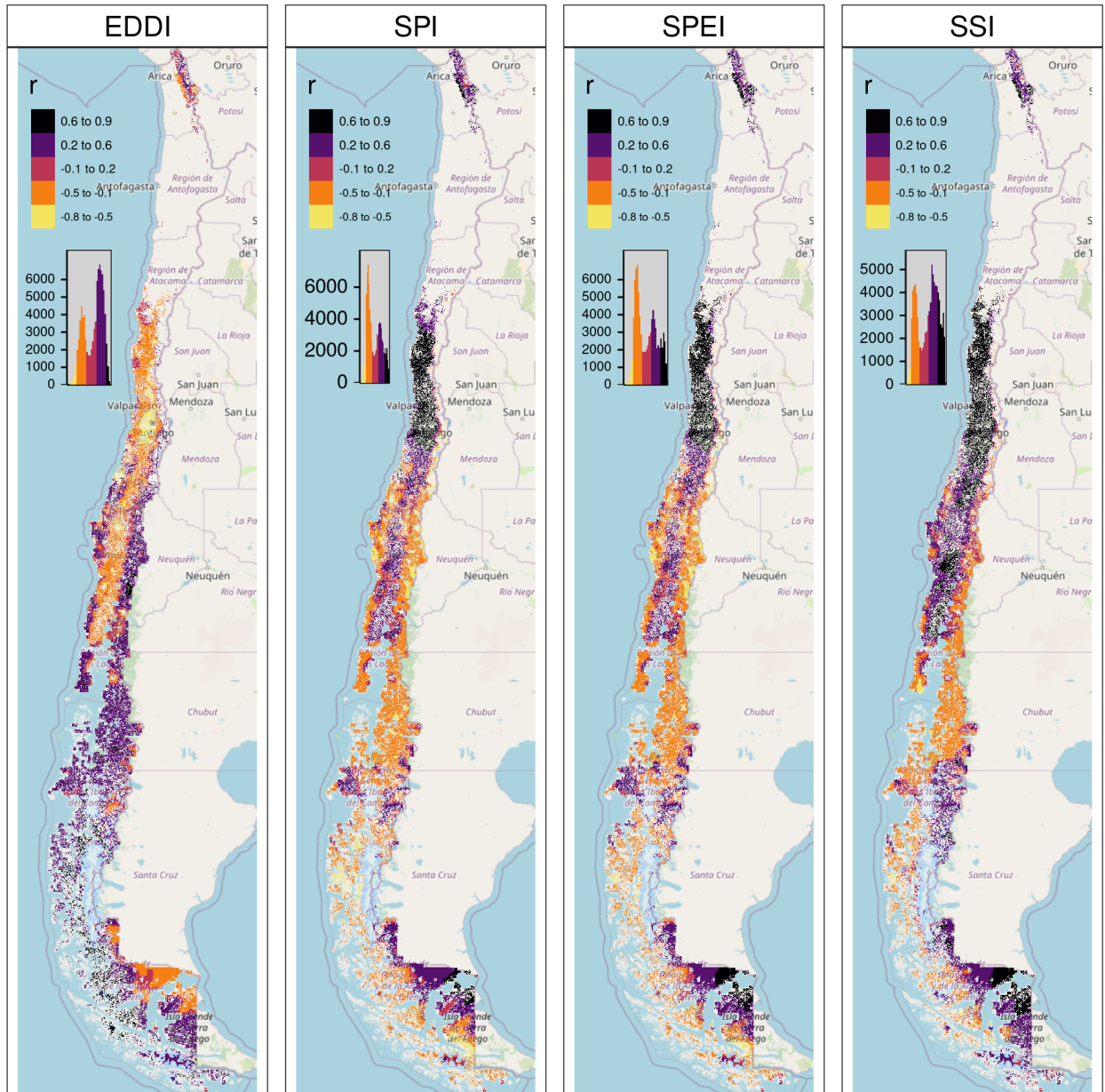


Figure 9: Pearson correlation value for the time scales and drought index that reach the maximum coefficient of determination. White spaces indicate no significant correlation.

12 is still the variable explaining more of the variation in vegetation productivity ( $R^2 = 0.45$  in “Centro” and 0.2 in “Sur”). In the case of croplands, the SPEI-12, SPI-36, and SSI-12 explain between 45% and 66% of the variability in “Norte Chico”. The type of land most impacted by climatic variation was shrubland, where soil moisture explained 59% and precipitation, 37%, in “Norte Chico” and “Centro”, with SSI-12 being the most relevant variable, then SPI-36 in “Norte Chico” and SPI-24 in “Sur”.

Table 5: Summary per land cover macroclass and macrozone regarding the correlation between zcNDVI with the drought indices EDDI, SPI, SPEI, and SSI for time scales of 1, 3, 6, 12, 24, and 36. The numbers in each cell indicate the time scale that reached the maximum correlation for the land cover and macrozone, and the color indicates the strength of the r-squared obtained with the index and the time scale. Cells without values indicate that the land cover type was not significant in that macrozone.

|              | Forest   |     |      |     | Cropland |     |      |     | Grassland |     |      |     | Savanna |     |      |     | Shrubland |     |      |     |  |  |
|--------------|--|-----|------|-----|----------|-----|------|-----|-----------|-----|------|-----|---------|-----|------|-----|-----------|-----|------|-----|--|--|
| Macrozone    | EDDI   | SPI | SPEI | SSI | EDDI     | SPI | SPEI | SSI | EDDI      | SPI | SPEI | SSI | EDDI    | SPI | SPEI | SSI | EDDI      | SPI | SPEI | SSI |  |  |
| Norte Grande |  |     |      |     |          |     |      |     | 36        | 36  | 36   | 12  |         |     |      |     | 36        | 12  | 36   | 12  |  |  |
| Norte Chico  |  |     |      |     | 36       | 36  | 12   | 12  | 36        | 36  | 24   | 12  | 36      | 24  | 24   | 12  | 36        | 36  | 24   | 12  |  |  |
| Centro       | 36   | 36  | 12   | 6   | 12       | 12  | 6    | 6   | 12        | 12  | 12   | 36  | 12      | 12  | 12   | 36  | 24        | 24  | 12   |     |  |  |
| Sur          | 36   |     |      |     |          | 6   | 6    | 6   | 6         | 6   | 6    | 6   | 6       | 6   | 6    | 6   | 6         |     |      |     |  |  |
| Austral      | 6  | 6   |      |     |          |     |      |     |           |     | 6    | 12  | 12      | 6   | 6    | 12  |           |     |      |     |  |  |
| r-squared    | <br>0.2 0.4 0.6 |     |      |     |          |     |      |     |           |     |      |     |         |     |      |     |           |     |      |     |  |  |

## 398 5. Discussion

### 399 5.1. Vegetation water demand and its relation to drought

400 In our study, we considered the variation in vegetation productivity in Chile, specifically in areas without any  
 401 changes in land cover, to prevent any misleading conclusions about the increase in water demand due to land  
 402 cover change. Our results show a contrasting perspective regarding the evidence provided by [Vicente-Serrano et al. \(2022\)](#), who indicates that the increase in drought is led by an increase in agricultural  
 403 land, which in turn increases water demand.

404 Our results indicate that except for the southern part of the country, the SPI, SPEI, and SSI (water supply)  
 405 showed declining trends, while the EDDI (water demand) increased across continental Chile. The trends in  
 406 water demand and supply were stronger as the time scales increased, indicating a long-term reduction in  
 407 water supply (except for the southern part) and an increase in water demand by the atmosphere. Also, we  
 408 found that there has been a significant declining trend in vegetation productivity (zcNDVI) since 2000 for  
 409 the north-central part of the country, which reached its lowest level between 2020 and 2022 and has impacted  
 410 natural and cultivated land. Further, croplands showed a decrease in surface area for the north-central region,  
 411 while barren land increased. We link these changes to a decrease in the water demand from vegetation  
 412 because, despite the increase in AED, the surface area for water-demanding vegetation is declining as well as  
 413 the biomass production. However, some questions arise regarding what is occurring with the cultivated land.  
 414 Evidence suggests that higher-water-demanding crops have replaced less demanding crops in the Petorca  
 415 basin (central Chile), leading to an increase in water abstraction ([Muñoz et al., 2020](#); [Duran-Llacer et al., 2020](#)).  
 416 Nonetheless, at this scale of analysis, the effect of higher crop water demand on drought is minor  
 417 compared to the decrease in water supply and increase in AED over all land cover types.

418 The long-scale trends (e.g., 36 months) demonstrate the impact of climate change on water availability in  
 419 Chile, potentially due to an intense hydrological drought stemming from the ongoing precipitation deficit  
 420 and rising AED. But it is likely that in zones most affected by drought, the main cause is not an increase in  
 421 vegetation water demand due to an intensification of cultivated land (e.g., an increase in irrigated crops) like  
 422 in other parts of the globe ([Vicente-Serrano et al., 2020](#)). North-central Chile has experienced a decline in  
 423 vegetation productivity across land cover types, which is primarily attributable to variations in water supply  
 424 and soil moisture. An increase in water demand, led by an increase in the surface area of irrigated crops or  
 425 the change to more water-demanding crops, could strengthen this trend, however, it escapes the scope of

427 this study. Future work should focus on the regions where the drought has been more severe and has a high  
428 proportion of irrigated crops to get insight on the real impact of irrigation on ecosystems in those zones.

429 *5.2. Sensitivity of land cover vegetation to short- and long-term drought*

430 We analyzed the time series of drought indices and vegetation productivity per land cover type. Our results  
431 indicate that forest is the type most resistant to drought, and shrublands, savannas, and croplands have  
432 higher sensitivities.

433 In their study in the Yangtze River Basin in China, [Jiang et al. \(2020\)](#) analyzed the impact of drought on  
434 vegetation using the SPEI and the Enhanced Vegetation Index (EVI). They found that cropland was more  
435 sensitive to drought than grassland, showing that cropland responds strongly to short- and medium-term  
436 drought (< SPEI-6). In our case, the SPEI-12 was the one that most impacted the croplands in “Norte  
437 Chico” and “Centro”. In general, most studies show that croplands are most sensitive to short-term drought  
438 (< SPI-6) ([Zambrano et al., 2016](#); [Potopová et al., 2015](#); [Dai et al., 2020](#); [Rhee et al., 2010](#)). Short-term  
439 precipitation deficits have an impact on soil water, so less water is available for plant growth. However,  
440 we found that in “Norte Chico”, an SPI-36 and SPEI-12 had a higher impact, which are associated with  
441 long-term water deficit, and in “Centro”, an SPI-12 and SPEI-12. Thus, we hypothesize that this impact  
442 could be attributed to the hydrological drought that has decreased groundwater storage ([Taucare et al.,](#)  
443 [2024](#)), which in turn is impacted by long-term deficits, and consequently, the vegetation is more dependent on  
444 groundwater. In “Sur” and “Austral”, the correlations between drought indices and vegetation productivity  
445 decrease, as do the time scales that reach the maximum r-squared. The possible reason for this is that the  
446 most resistant types, forest and grassland, predominate south of “Centro”. Also, drought episodes have been  
447 less frequent and intense and have had a lower impact on water availability for vegetation.

448 In central Chile, [Venegas-González et al. \(2023\)](#) observed a significant decline in the overall growth of  
449 sclerophyllous moist forests (mediterranean forests), which they attributed to increased drought conditions.  
450 However, we found that forests are the most resilient land cover class to drought, with less variation in  
451 drought indices. In the “Sur”, there is a large domain of planted forests that have replaced native vegetation  
452 since the 1970s ([Heilmayr et al., 2016, 2020](#); [Miranda et al., 2017](#)), impacting biodiversity and ecosystem  
453 services ([Rodríguez-Echeverry et al., 2018](#)). It has recently been shown that these planted forests are  
454 responding positively to climate change, and it is expected that they will benefit from future climate scenarios  
455 ([Carrasco et al., 2022](#)). Further, the forests of the “Austral” region correspond to Patagonian ecosystems,  
456 mainly native forests dominated by tree species of wide niche breadth . Overall, these forests have been  
457 more affected by the increase in temperature than by the reduction in moisture ([Fajardo et al., 2023](#); [Holz](#)  
458 [et al., 2018](#)). These responses have caused stabilized tree growth, linked to more frequent warm autumns  
459 ([Gibson-Carpintero et al., 2022](#)). It has also been observed that these forests have shown resistance to drought  
460 episodes ([Fajardo et al., 2023](#)), which might be attributable to their relatively low growth rate. Supporting  
461 this is [Fathi-Taperasht et al. \(2022\)](#), who assert that Indian forests are the most drought-resistant and recover  
462 rapidly. Similarly, the work of [Wu et al. \(2024\)](#), who analyzed vegetation loss and recovery in response to  
463 meteorological drought in the humid subtropical Pearl River basin in China, indicates that forests showed  
464 higher drought resistance. Using Vegetation Optical Depth (VOD), kNDVI, and EVI, [Xiao et al. \(2023\)](#)  
465 tested the resistance of ecosystems and found that ecosystems with more forests are better able to handle  
466 severe droughts than croplands. They attribute the difference to a deeper rooting depth for trees, a higher  
467 water storage capacity, and different water use strategies between forest and cropland ([Xiao et al., 2023](#)).

468 In another study, [Fuentes et al. \(2021\)](#) evaluated water scarcity and land cover change in Chile between 29°  
469 and 39° south latitude. They used the one-month SPEI for drought evaluation, which resulted in misleading  
470 results. For instance, they failed to identify a temporal trend in the SPEI, but they still observed a decline  
471 in water availability and a rise in AED, trends that should have been detectable if they were using longer  
472 SPEI time scales. Thus, according to the results presented in this study, for the assessment of drought, it is  
473 necessary to consider drought indices on a short- to long-scale basis.

474    *5.3. Vegetation productivity and drought*

475    We found that the 12-month soil moisture deficit affected plant productivity in all land cover types in Chile.  
476    The main external factors that affect biomass production by vegetation are actual evapotranspiration and soil  
477    moisture, and the rate of ET in turn depends on the availability of water storage in the root zone. Thus, soil  
478    moisture plays a key role in land carbon uptake and, consequently, in the production of biomass (Humphrey  
479    et al., 2021). The study results showed that the soil moisture-based drought index (SSI) was better at  
480    explaining vegetation productivity across land cover macroclasses than meteorological drought indices like  
481    SPI, SPEI, and EDDI. According to (Chatterjee et al., 2022) in the early growing season and especially in  
482    irrigated rather than rainfed croplands, soil moisture has better skills than SPI and SPEI for estimating gross  
483    primary production (GPP). Also, Zhou et al. (2021) indicate that the monthly scaled Standardized Water  
484    Deficit Index (SWDI) can accurately show the effects of agricultural drought in most of China. Nicolai-Shaw  
485    et al. (2017) also looked at the time-lag between the SWDI and the Vegetation Condition Index (VCI). They  
486    found that there was little to no time-lag in croplands but a greater time-lag in forests.

487    In our case, there is strong spatial variability throughout Chile and between classes, mainly attributable to  
488    climate heterogeneity, hydrological status, or vegetation resistance to water scarcity. The semi-arid “Norte  
489    Chico” and the Mediterranean “Centro” were where SSI had the best performance. In Chile, medium-term  
490    deficits of 12 months are more relevant in the response of vegetation for all land cover types, which decreases  
491    to the south, and in the case of croplands, they seem to react in a shorter time, with six months (SSI-6) in  
492    “Centro”. This variation for croplands could be related to the fact that in “Norte Chico”, the majority of crops  
493    are irrigated, but to the south there is a higher proportion of rainfed agriculture, which is most dependent on  
494    the short-term availability of water. Rather, in “Norte Chico”, the orchards are more dependent on irrigation,  
495    which in turn depends on the availability of storage water in dams or groundwater reservoirs, which are  
496    affected by long-term drought (e.g., SPI-36).

497    *5.4. Drought information to aid in adaptation*

498    Our findings present valuable information for policymakers in developing adaptation strategies for droughts.  
499    Our results show that the different climate components, such as AED, water supply, soil moisture, and  
500    their impact on vegetation, should be considered when evaluating the multi-dimensional nature of drought.  
501    Also, for a better understanding of drought propagation (Van Loon et al., 2012) from meteorological to  
502    agricultural and ecological drought, we should consider the climatic response at different time scales, ranging  
503    from short to long. Additionally, the spatiotemporal characteristics of our results allow us to distinguish  
504    distinct geographical contexts, recognizing the diversity in climate, but also shedding light on agricultural  
505    practices (ranging from irrigated to dryland farming), technological advancements in irrigation efficiency,  
506    and the region-specific capabilities for drought adaptation, including groundwater management and reservoir  
507    water storage. This information, combined with agricultural information and statistics, could provide a  
508    strong foundation for the development of science-based adaptation policies.

509    In a commitment to fostering informed and dynamic adaptation efforts, our results are disseminated  
510    publicly and continually updated via the Drought Observatory for Agriculture and Biodiversity of Chile  
511    (ODES) <https://odes-chile.org/app/unidades> (Zambrano, 2023a; Kunst and Zambrano, 2023). This initiative  
512    ensures the availability and easy accessibility of extensive climate data, facilitating the development of  
513    adaptive strategies that are both responsive to the realities of different regions and grounded in the latest  
514    scientific understanding. The proactive sharing and updating of such data underscores its key role in enabling  
515    policymakers to craft adaptive measures that are finely tuned to the diverse and evolving landscapes of  
516    drought impacts. Furthermore, the recently promulgated law about climate change in Chile (Law 21.455,  
517    <https://www.bcn.cl/leychile/navegar?idNorma=1177286>), which aims to implement sectoral adaptation plans  
518    for agriculture, forests, and biodiversity, could benefit from this information.

519    **6. Conclusion**

520    We found a significant trend toward decreasing water supply (SPI, SPEI, and SSI) in most of the Chilean  
521    territory, with the exception of the southern region. The trend is the strongest in the north-central zone. The

whole country showed an increase in water demand (AED) due to increasing temperatures. The magnitude of the trends is stronger for longer time scales, which is evidence that there is a prolonged precipitation shortage and a prolonged increase in AED. The trend in vegetation productivity in the north-central area is affecting shrubland and savanna to a greater degree, followed by croplands and forests.

Using Random Forest and variable importance metrics, we assessed how land cover trends relate to drought indices and found that drought indices across Chile could explain about 12–41% of the trends in land cover types. Drought explains a higher variance in changes in shrublands, followed by savanna, grasslands, and forest. The changes in croplands showed the lowest association with drought. We found that the short- to long-term trend in AED was the most important variable that could partially explain the observed land cover trend, followed by long-term trends in precipitation and short-term trends in soil moisture.

The trends in drought indices are accompanied by multiple land cover changes in the country, most notably an increase of forest in “Sur”, of shrubland and grassland in “Centro”, and of savanna in “Centro” and “Sur”. In “Norte Chico” and “Centro”, the croplands have been declining in surface, whereas in “Sur”, there is an increase in cultivated land.

The change in vegetation productivity has been severe in the north-central part of the country for all land cover types, particularly savanna, shrubland, and croplands. The anomaly in soil moisture over the past 12 months is the main variable explaining these changes, followed by anomalies in accumulated precipitation over one to two years. The variation in AED is likely to exacerbate the drought’s impact on vegetation productivity.

The results of this study provide insightful information that can assist in developing adaptation measures for Chilean ecosystems to cope with climate change and drought. This information could be used in the scope of the national law on climate change, which seeks to implement adaptation strategies for agriculture, forests, and biodiversity.

## 7. Acknowledgment

The National Research and Development Agency of Chile (ANID) funded this study through the drought emergency project FSEQ210022, Fondecyt Iniciación N°11190360, Fondecyt Postdoctorado N°3230678, and Fondecyt Regular N°1210526.

## References

- Abramowitz, M., Stegun, I.A., 1968. Handbook of mathematical functions with formulas, graphs, and mathematical tables. volume 55. US Government printing office.
- Aceituno, P., Boisier, J.P., Garreaud, R., Rondanelli, R., Ruttlant, J.A., 2021. Climate and Weather in Chile, in: Fernández, B., Gironás, J. (Eds.), Water Resources of Chile. Springer International Publishing, Cham. volume 8, pp. 7–29. URL: [http://link.springer.com/10.1007/978-3-030-56901-3\\_2](http://link.springer.com/10.1007/978-3-030-56901-3_2).
- AghaKouchak, A., 2014. A baseline probabilistic drought forecasting framework using standardized soil moisture index: application to the 2012 United States drought. *Hydrology and Earth System Sciences* 18, 2485–2492. URL: <https://hess.copernicus.org/articles/18/2485/2014/>, doi:[10.5194/hess-18-2485-2014](https://doi.org/10.5194/hess-18-2485-2014).
- AghaKouchak, A., Mirchi, A., Madani, K., Di Baldassarre, G., Nazemi, A., Alborzi, A., Anjileli, H., Azarderakhsh, M., Chiang, F., Hassanzadeh, E., Huning, L.S., Mallakpour, I., Martinez, A., Mazdiyasni, O., Moftakhari, H., Norouzi, H., Sadegh, M., Sadeqi, D., Van Loon, A.F., Wanders, N., 2021. Anthropogenic Drought: Definition, Challenges, and Opportunities. *Reviews of Geophysics* 59, e2019RG000683. URL: <https://agupubs.onlinelibrary.wiley.com/doi/10.1029/2019RG000683>, doi:[10.1029/2019RG000683](https://doi.org/10.1029/2019RG000683).
- Akinyemi, F.O., 2021. Vegetation Trends, Drought Severity and Land Use-Land Cover Change during the Growing Season in Semi-Arid Contexts. *Remote Sensing* 2021, Vol. 13, Page 836 13, 836. URL: <https://www.mdpi.com/2072-4292/13/5/836/htm>, doi:[10.3390/RS13050836](https://doi.org/10.3390/RS13050836). publisher: Multidisciplinary Digital Publishing Institute.
- Alvarez-Garreton, C., Boisier, J.P., Garreaud, R., Seibert, J., Vis, M., 2021. Progressive water deficits during multiyear droughts in basins with long hydrological memory in Chile. *Hydrology and Earth System Sciences* 25, 429–446. URL: <https://hess.copernicus.org/articles/25/429/2021/>, doi:[10.5194/hess-25-429-2021](https://doi.org/10.5194/hess-25-429-2021).
- Bakker, K., 2012. Water Security: Research Challenges and Opportunities. *Science* 337, 914–915. URL: <https://www.science.org/doi/10.1126/science.1226337>, doi:[10.1126/science.1226337](https://doi.org/10.1126/science.1226337).

- 571 Barría, P., Sandoval, I.B., Guzman, C., Chadwick, C., Alvarez-Garreton, C., Díaz-Vasconcellos, R., Ocampo-Melgar, A.,  
 572 Fuster, R., 2021. Water allocation under climate change. *Elementa: Science of the Anthropocene* 9, 00131. URL:  
 573 <https://online.ucpress.edu/elementa/article/9/1/00131/117183/Water-allocation-under-climate-changeA-diagnosis>, doi:10.  
 574 1525/elementa.2020.00131.
- 575 Beck, H.E., McVicar, T.R., Vergopolan, N., Berg, A., Lutsko, N.J., Dufour, A., Zeng, Z., Jiang, X., van Dijk, A.I.J.M., Miralles,  
 576 D.G., 2023. High-resolution (1 km) Köppen-Geiger maps for 1901–2099 based on constrained CMIP6 projections. *Scientific  
 577 Data* 10. URL: <http://dx.doi.org/10.1038/s41597-023-02549-6>, doi:10.1038/s41597-023-02549-6.
- 578 Beguería, S., Vicente-Serrano, S.M., 2023. SPEI: Calculation of the Standardized Precipitation-Evapotranspiration Index. URL:  
 579 <https://CRAN.R-project.org/package=SPEI>.
- 580 Boisier, J.P., Alvarez-Garreton, C., Cordero, R.R., Damiani, A., Gallardo, L., Garreaud, R.D., Lambert, F., Ramallo, C.,  
 581 Rojas, M., Rondanelli, R., 2018. Anthropogenic drying in central-southern Chile evidenced by long-term observations  
 582 and climate model simulations. *Elementa* 6, 74. URL: <https://www.elementascience.org/article/10.1525/elementa.328>,  
 583 doi:10.1525/elementa.328.
- 584 Calvin, K., Dasgupta, D., Krinner, G., Mukherji, A., Thorne, P.W., Trisos, C., Romero, J., Aldunce, P., Barrett, K., Blanco,  
 585 G., Cheung, W.W., Connors, S., Denton, F., Diongue-Niang, A., Dodman, D., Garschagen, M., Geden, O., Hayward, B.,  
 586 Jones, C., Jotzo, F., Krug, T., Lasco, R., Lee, Y.Y., Masson-Delmotte, V., Meinshausen, M., Mintenbeck, K., Mokssit, A.,  
 587 Otto, F.E., Pathak, M., Pirani, A., Poloczanska, E., Pörtner, H.O., Revi, A., Roberts, D.C., Roy, J., Ruane, A.C., Skea,  
 588 J., Shukla, P.R., Slade, R., Slangen, A., Sokona, Y., Sörensson, A.A., Tignor, M., Van Vuuren, D., Wei, Y.M., Winkler,  
 589 H., Zhai, P., Zommers, Z., Hourcade, J.C., Johnson, F.X., Pachauri, S., Simpson, N.P., Singh, C., Thomas, A., Totin, E.,  
 590 Arias, P., Bustamante, M., Elgizouli, I., Flato, G., Howden, M., Méndez-Vallejo, C., Pereira, J.J., Pichs-Madruga, R., Rose,  
 591 S.K., Saheb, Y., Sánchez Rodríguez, R., Ürge Vorsatz, D., Xiao, C., Yassaa, N., Alegría, A., Armour, K., Bednar-Friedl, B.,  
 592 Blok, K., Cissé, G., Dentener, F., Eriksen, S., Fischer, E., Garner, G., Guivarch, C., Haasnoot, M., Hansen, G., Hauser, M.,  
 593 Hawkins, E., Hermans, T., Kopp, R., Leprince-Ringuet, N., Lewis, J., Ley, D., Ludden, C., Niamir, L., Nicholls, Z., Some, S.,  
 594 Szopa, S., Trewin, B., Van Der Wijst, K.I., Winter, G., Witting, M., Birt, A., Ha, M., Romero, J., Kim, J., Haines, E.F.,  
 595 Jung, Y., Stavins, R., Birt, A., Ha, M., Orendain, D.J.A., Ignon, L., Park, S., Park, Y., Reisinger, A., Cammaramo, D.,  
 596 Fischlin, A., Fuglestvedt, J.S., Hansen, G., Ludden, C., Masson-Delmotte, V., Matthews, J.R., Mintenbeck, K., Pirani, A.,  
 597 Poloczanska, E., Leprince-Ringuet, N., Péan, C., 2023. IPCC, 2023: Climate Change 2023: Synthesis Report. Contribution  
 598 of Working Groups I, II and III to the Sixth Assessment Report of the Intergovernmental Panel on Climate Change [Core  
 599 Writing Team, H. Lee and J. Romero (eds.)]. IPCC, Geneva, Switzerland. Technical Report. Intergovernmental Panel on  
 600 Climate Change (IPCC). URL: <https://www.ipcc.ch/report/ar6/syr/>.
- 601 Camps-Valls, G., Campos-Taberner, M., Moreno-Martínez, , Walther, S., Duveiller, G., Cescatti, A., Mahecha, M.D., Muñoz-  
 602 Marí, J., García-Haro, F.J., Guanter, L., Jung, M., Gamon, J.A., Reichstein, M., Running, S.W., 2021. A unified vegetation  
 603 index for quantifying the terrestrial biosphere. *Science Advances* 7, eabc7447. URL: <https://www.science.org/doi/10.1126/sciadv.abc7447>, doi:10.1126/sciadv.abc7447.
- 604 Carrasco, G., Almeida, A.C., Falvey, M., Olmedo, G.F., Taylor, P., Santibañez, F., Coops, N.C., 2022. Effects of climate change  
 605 on forest plantation productivity in Chile. *Global Change Biology* 28, 7391–7409. URL: <https://onlinelibrary.wiley.com/doi/10.1111/gcb.16418>, doi:10.1111/gcb.16418.
- 606 Chamlng, M., Bera, B., 2020. Spatio-temporal Patterns of Land Use/Land Cover Change in the Bhutan–Bengal Foothill Region  
 607 Between 1987 and 2019: Study Towards Geospatial Applications and Policy Making. *Earth Systems and Environment* 4,  
 608 117–130. URL: <http://link.springer.com/10.1007/s41748-020-00150-0>, doi:10.1007/s41748-020-00150-0.
- 609 Chatterjee, S., Desai, A.R., Zhu, J., Townsend, P.A., Huang, J., 2022. Soil moisture as an essential component for delineating  
 610 and forecasting agricultural rather than meteorological drought. *Remote Sensing of Environment* 269, 112833. URL:  
 611 <https://linkinghub.elsevier.com/retrieve/pii/S0034425721005538>, doi:10.1016/j.rse.2021.112833.
- 612 Chen, J., Shao, Z., Huang, X., Zhuang, Q., Dang, C., Cai, B., Zheng, X., Ding, Q., 2022. Assessing the impact of drought-land  
 613 cover change on global vegetation greenness and productivity. *Science of The Total Environment* 852, 158499. URL:  
 614 <https://linkinghub.elsevier.com/retrieve/pii/S004896972205598X>, doi:10.1016/j.scitotenv.2022.158499.
- 615 Cheng, Y., Oehmcke, S., Brandt, M., Rosenthal, L., Das, A., Vrieling, A., Saatchi, S., Wagner, F., Mugabowindekwe, M.,  
 616 Verbruggen, W., Beier, C., Horion, S., 2024. Scattered tree death contributes to substantial forest loss in California. *Nature  
 617 Communications* 15, 641. URL: <https://www.nature.com/articles/s41467-024-44991-z>, doi:10.1038/s41467-024-44991-z.
- 618 Crausbay, S.D., Ramirez, A.R., Carter, S.L., Cross, M.S., Hall, K.R., Bathke, D.J., Betancourt, J.L., Colt, S., Cravens,  
 619 A.E., Dalton, M.S., Dunham, J.B., Hay, L.E., Hayes, M.J., McEvoy, J., McNutt, C.A., Moritz, M.A., Nislow, K.H.,  
 620 Raheem, N., Sanford, T., 2017. Defining Ecological Drought for the Twenty-First Century. *Bulletin of the American  
 621 Meteorological Society* 98, 2543–2550. URL: <https://journals.ametsoc.org/view/journals/bams/98/12/bams-d-16-0292.1.xml>,  
 622 doi:10.1175/BAMS-D-16-0292.1. publisher: American Meteorological Society.
- 623 Dai, M., Huang, S., Huang, Q., Leng, G., Guo, Y., Wang, L., Fang, W., Li, P., Zheng, X., 2020. Assessing agricultural drought  
 624 risk and its dynamic evolution characteristics. *Agricultural Water Management* 231, 106003. URL: [https://linkinghub.elsevier.com/retrieve/pii/S0378377419316531](https://linkinghub.elsevier.<br/>
  625 com/retrieve/pii/S0378377419316531), doi:10.1016/j.agwat.2020.106003.
- 626 Didan, K., 2015. MOD13Q1 MODIS/Terra Vegetation Indices 16-Day L3 Global 250m SIN Grid V006. Technical Report.  
 627 NASA EOSDIS Land Processes DAAC. doi:<http://dx.doi.org/10.5067/MODIS/MOD13Q1.006>.
- 628 Duran-Llacer, I., Munizaga, J., Arumí, J., Ruybal, C., Aguayo, M., Sáez-Carrillo, K., Arriagada, L., Rojas, O., 2020. Lessons to  
 629 Be Learned: Groundwater Depletion in Chile's Ligua and Petorca Watersheds through an Interdisciplinary Approach. *Water*  
 630 12, 2446. URL: <https://www.mdpi.com/2073-4441/12/9/2446>, doi:10.3390/w12092446.
- 631 Echeverría, C., Newton, A., Nahuelhual, L., Coomes, D., Rey-Benayas, J.M., 2012. How landscapes change: Integration of  
 632 spatial patterns and human processes in temperate landscapes of southern Chile. *Applied Geography* 32, 822–831. URL:  
 633 <https://linkinghub.elsevier.com/retrieve/pii/S0143622811001676>, doi:10.1016/j.apgeog.2011.08.014.

- 636 Fajardo, A., Gazol, A., Meynard, P.M., Mayr, C., Martínez Pastur, G.J., Peri, P.L., Camarero, J.J., 2023. Climate change-related  
 637 growth improvements in a wide niche-breadth tree species across contrasting environments. *Annals of Botany* 131, 941–951.  
 638 URL: <https://academic.oup.com/aob/article/131/6/941/7095679>, doi:10.1093/aob/mcad053.
- 639 FAO, 2022. The State of the World's Forests 2022. FAO. URL: <http://www.fao.org/documents/card/en/c/cb9360en>.
- 640 Farahmand, A., AghaKouchak, A., 2015. A generalized framework for deriving nonparametric standardized drought indicators.  
 641 *Advances in Water Resources* 76, 140–145. URL: <https://linkinghub.elsevier.com/retrieve/pii/S0309170814002322>, doi:10.  
 642 1016/j.advwatres.2014.11.012.
- 643 Fathi-Taperasht, A., Shafizadeh-Moghadam, H., Minaei, M., Xu, T., 2022. Influence of drought duration and severity on drought  
 644 recovery period for different land cover types: evaluation using MODIS-based indices. *Ecological Indicators* 141, 109146.  
 645 URL: <https://linkinghub.elsevier.com/retrieve/pii/S1470160X22006185>, doi:10.1016/j.ecolin.2022.109146.
- 646 Ford, T.W., Otkin, J.A., Quiring, S.M., Lisonbee, J., Woloszyn, M., Wang, J., Zhong, Y., 2023. Flash Drought Indicator  
 647 Intercomparison in the United States. *Journal of Applied Meteorology and Climatology* 62, 1713–1730. URL: <https://journals.ametsoc.org/view/journals/apme/62/12/JAMC-D-23-0081.1.xml>, doi:10.1175/JAMC-D-23-0081.1.
- 648 Fuentes, I., Fuster, R., Avilés, D., Vervoort, W., 2021. Water scarcity in central Chile: the effect of climate and land cover  
 649 changes on hydrologic resources. *Hydrological Sciences Journal* 66, 1028–1044. URL: <https://www.tandfonline.com/doi/full/10.1080/02626667.2021.1903475>, doi:10.1080/02626667.2021.1903475.
- 650 Garreaud, R., Alvarez-Garreton, C., Barichivich, J., Boisier, J.P., Christie, D., Galleguillos, M., LeQuesne, C., McPhee, J.,  
 651 Zambrano-Bigiarini, M., 2017. The 2010–2015 mega drought in Central Chile: Impacts on regional hydroclimate and vegetation.  
 652 *Hydrology and Earth System Sciences Discussions* 2017, 1–37. URL: <http://www.hydrol-earth-syst-sci-discuss.net/hess-2017-191/>, doi:10.5194/hess-2017-191.
- 653 Garreaud, R.D., 2009. The Andes climate and weather. *Advances in Geosciences* 22, 3–11. URL: <https://adgeo.copernicus.org/articles/22/3/2009/>, doi:10.5194/adgeo-22-3-2009.
- 654 Gebrechorkos, S.H., Peng, J., Dyer, E., Miralles, D.G., Vicente-Serrano, S.M., Funk, C., Beck, H.E., Asfaw, D.T., Singer, M.B.,  
 655 Dadson, S.J., 2023. Global high-resolution drought indices for 1981–2022. *Earth System Science Data* 15, 5449–5466. URL:  
 656 <https://essd.copernicus.org/articles/15/5449/2023/>, doi:10.5194/essd-15-5449-2023.
- 657 Gibson-Carpintero, S., Venegas-González, A., Urrea, V.D., Estay, S.A., Gutiérrez, G., 2022. Recent increase in autumn  
 658 temperature has stabilized tree growth in forests near the tree lines in Chilean Patagonia. *Ecosphere* 13, e4266. URL:  
 659 <https://esajournals.onlinelibrary.wiley.com/doi/10.1002/ecs2.4266>, doi:10.1002/ecs2.4266.
- 660 Hao, Z., AghaKouchak, A., 2013. Multivariate Standardized Drought Index: A parametric multi-index model. *Advances in Water  
 661 Resources* 57, 12–18. URL: <https://linkinghub.elsevier.com/retrieve/pii/S0309170813000493>, doi:10.1016/j.advwatres.2013.03.009.
- 662 Hargreaves, G.H., 1994. Defining and Using Reference Evapotranspiration. *Journal of Irrigation and Drainage Engineering*  
 663 120, 1132–1139. URL: <https://ascelibrary.org/doi/10.1061/%28ASCE%290733-9437%281994%29120%3A6%281132%29>,  
 664 doi:10.1061/(ASCE)0733-9437(1994)120:6(1132).
- 665 Hargreaves, G.H., Samani, Z.A., 1985. Reference crop evapotranspiration from temperature. *Applied engineering in agriculture*  
 666 1, 96–99.
- 667 Heilmayr, R., Echeverría, C., Fuentes, R., Lambin, E.F., 2016. A plantation-dominated forest transition in Chile. *Applied  
 668 Geography* 75, 71–82. URL: <https://linkinghub.elsevier.com/retrieve/pii/S0143622816302600>, doi:10.1016/j.apgeog.2016.07.014.
- 669 Heilmayr, R., Echeverría, C., Lambin, E.F., 2020. Impacts of Chilean forest subsidies on forest cover, carbon and biodiversity.  
 670 *Nature Sustainability* 3, 701–709. URL: <https://www.nature.com/articles/s41893-020-0547-0>, doi:10.1038/s41893-020-0547-0.
- 671 Heim, R.R., 2002. A Review of Twentieth-Century Drought Indices Used in the United States. *Bulletin of the American  
 672 Meteorological Society* 83, 1149–1166. URL: <https://journals.ametsoc.org/doi/10.1175/1520-0477-83.8.1149>, doi:10.1175/  
 673 1520-0477-83.8.1149.
- 674 Helman, D., Mussery, A., Lensky, I.M., Leu, S., 2014. Detecting changes in biomass productivity in a different land management  
 675 regimes in drylands using satellite-derived vegetation index. *Soil Use and Management* 30, 32–39. URL: <https://bsssjournals.onlinelibrary.wiley.com/doi/10.1111/sum.12099>, doi:10.1111/sum.12099.
- 676 Hijmans, R.J., 2023. terra: Spatial Data Analysis. URL: <https://CRAN.R-project.org/package=terra>.
- 677 Ho, T.K., 1995. Random decision forests, in: Proceedings of 3rd international conference on document analysis and recognition,  
 678 IEEE. pp. 278–282.
- 679 Hobbins, M.T., Wood, A., McEvoy, D.J., Huntington, J.L., Morton, C., Anderson, M., Hain, C., 2016. The Evaporative Demand  
 680 Drought Index. Part I: Linking Drought Evolution to Variations in Evaporative Demand. *Journal of Hydrometeorology* 17,  
 681 1745–1761. URL: <https://journals.ametsoc.org/doi/10.1175/JHM-D-15-0121.1>, doi:10.1175/JHM-D-15-0121.1.
- 682 Holz, A., Hart, S.J., Williamson, G.J., Veblen, T.T., Aravena, J.C., 2018. Radial growth response to climate change along the  
 683 latitudinal range of the world's southernmost conifer in southern South America. *Journal of Biogeography* 45, 1140–1152.  
 684 URL: <https://onlinelibrary.wiley.com/doi/10.1111/jbi.13199>, doi:10.1111/jbi.13199.
- 685 Homer, C., Dewitz, J., Jin, S., Xian, G., Costello, C., Danielson, P., Gass, L., Funk, M., Wickham, J., Stehman, S., Auch, R.,  
 686 Riitters, K., 2020. Conterminous United States land cover change patterns 2001–2016 from the 2016 National Land Cover  
 687 Database. *ISPRS Journal of Photogrammetry and Remote Sensing* 162, 184–199. URL: <https://linkinghub.elsevier.com/retrieve/pii/S0924271620300587>, doi:10.1016/j.isprsjprs.2020.02.019.
- 688 Hufkens, K., Stauffer, R., Campitelli, E., 2019. The ecwmfr package: an interface to ECMWF API endpoints. URL:  
 689 <https://bluegreen-labs.github.io/ecmwfr/>.
- 690 Humphrey, V., Berg, A., Ciais, P., Gentine, P., Jung, M., Reichstein, M., Seneviratne, S.I., Frankenberg, C., 2021. Soil  
 691 moisture–atmosphere feedback dominates land carbon uptake variability. *Nature* 592, 65–69. URL: <https://www.nature.com/doi/10.1038/s41586-021-03537-w>

- 701       articles/s41586-021-03325-5, doi:10.1038/s41586-021-03325-5.
- 702 IPCC, 2013. Climate Change 2013: The Physical Science Basis. Contribution of Working Group I to the Fifth Assessment  
703 Report of the Intergovernmental Panel on Climate Change. Cambridge University Press, Cambridge, UK; New York, USA.  
704 URL: [www.climatechange2013.org](http://www.climatechange2013.org), doi:10.1017/CBO9781107415324.
- 705 Jiang, W., Wang, L., Feng, L., Zhang, M., Yao, R., 2020. Drought characteristics and its impact on changes in surface  
706 vegetation from 1981 to 2015 in the Yangtze River Basin, China. International Journal of Climatology 40, 3380–3397. URL:  
707 <https://rmets.onlinelibrary.wiley.com/doi/10.1002/joc.6403>, doi:10.1002/joc.6403.
- 708 Kendall, M., 1975. Rank correlation methods (4th ed. 2d impression). Griffin.
- 709 Kogan, F., Guo, W., Yang, W., 2020. Near 40-year drought trend during 1981–2019 earth warming and food security. Geomatics,  
710 Natural Hazards and Risk 11, 469–490. URL: <https://www.tandfonline.com/doi/full/10.1080/19475705.2020.1730452>,  
711 doi:10.1080/19475705.2020.1730452.
- 712 Kuhn, M., Wickham, H., 2020. Tidymodels: a collection of packages for modeling and machine learning using tidyverse  
713 principles. URL: <https://www.tidymodels.org>.
- 714 Kunst, J., Zambrano, F., 2023. ODES Estaciones. URL: <https://zenodo.org/record/8189816>.
- 715 Laimighofer, J., Laaha, G., 2022. How standard are standardized drought indices? Uncertainty components for the SPI  
716 & SPEI case. Journal of Hydrology 613, 128385. URL: <https://linkinghub.elsevier.com/retrieve/pii/S0022169422009544>,  
717 doi:10.1016/j.jhydrol.2022.128385.
- 718 Li, H., Choy, S., Zaminpardaz, S., Wang, X., Liang, H., Zhang, K., 2024. Flash drought monitoring using diurnal-provided  
719 evaporative demand drought index. Journal of Hydrology 633, 130961. URL: <https://linkinghub.elsevier.com/retrieve/pii/S002216942400355X>, doi:10.1016/j.jhydrol.2024.130961.
- 720 Li, W., Migliavacca, M., Forkel, M., Denissen, J.M.C., Reichstein, M., Yang, H., Duveiller, G., Weber, U., Orth, R., 2022.  
721 Widespread increasing vegetation sensitivity to soil moisture. Nature Communications 13, 3959. URL: <https://www.nature.com/articles/s41467-022-31667-9>, doi:10.1038/s41467-022-31667-9.
- 722 Liu, X., Yu, S., Yang, Z., Dong, J., Peng, J., 2024. The first global multi-timescale daily SPEI dataset from 1982 to 2021.  
723 Scientific Data 11, 223. URL: <https://www.nature.com/articles/s41597-024-03047-z>, doi:10.1038/s41597-024-03047-z.
- 724 Luebert, F., Pliscoff, P., 2022. The vegetation of Chile and the EcoVeg approach in the context of the International  
725 Vegetation Classification project. Vegetation Classification and Survey 3, 15–28. URL: <https://vcs.pensoft.net/article/67893/>,  
726 doi:10.3897/VCS.67893.
- 727 Luysaert, S., Jammet, M., Stoy, P.C., Estel, S., Pongratz, J., Ceschia, E., Churkina, G., Don, A., Erb, K., Ferlicq, M.,  
728 Gielen, B., Grünwald, T., Houghton, R.A., Klumpp, K., Knohl, A., Kolb, T., Kuemmerle, T., Laurila, T., Lohila, A.,  
729 Loustau, D., McGrath, M.J., Meyfroidt, P., Moors, E.J., Naudts, K., Novick, K., Otto, J., Pilegaard, K., Pio, C.A., Rambal,  
730 S., Rebmann, C., Ryder, J., Suyker, A.E., Varlagin, A., Wattenbach, M., Dolman, A.J., 2014. Land management and  
731 land-cover change have impacts of similar magnitude on surface temperature. Nature Climate Change 4, 389–393. URL:  
732 <https://www.nature.com/articles/nclimate2196>, doi:10.1038/nclimate2196.
- 733 Masson-Delmotte, V., P.Z.A.P.S.L.C.C.P.S.B.N.C.Y.C.L.G.M.I.G.M.H.K.L.E.L.J.B.R.M.T.K.M.T.W.O.Y.R.Y.a.B.Z.e., 2021.  
734 IPCC, 2021: Climate Change 2021: The Physical Science Basis. Contribution of Working Group I to the Sixth Assessment  
735 Report of the Intergovernmental Panel on Climate Change. Technical Report. URL: <https://www.ipcc.ch/>. publication Title:  
736 Cambridge University Press. In Press.
- 737 McEvoy, D.J., Huntington, J.L., Hobbins, M.T., Wood, A., Morton, C., Anderson, M., Hain, C., 2016. The Evaporative Demand  
738 Drought Index. Part II: CONUS-Wide Assessment against Common Drought Indicators. Journal of Hydrometeorology 17,  
739 1763–1779. URL: <http://journals.ametsoc.org/doi/10.1175/JHM-D-15-0122.1>, doi:10.1175/JHM-D-15-0122.1.
- 740 Meroni, M., Rembold, F., Fasbender, D., Vrieling, A., 2017. Evaluation of the Standardized Precipitation Index as an  
741 early predictor of seasonal vegetation production anomalies in the Sahel. Remote Sensing Letters 8, 301–310. URL:  
742 <http://www.tandfonline.com/doi/abs/10.1080/2150704X.2016.1264020>, doi:10.1080/2150704X.2016.1264020.
- 743 Miranda, A., Altamirano, A., Cayuela, L., Lara, A., González, M., 2017. Native forest loss in the Chilean biodiversity hotspot:  
744 revealing the evidence. Regional Environmental Change 17, 285–297. URL: <http://link.springer.com/10.1007/s10113-016-1010-7>, doi:10.1007/s10113-016-1010-7.
- 745 Miranda, A., Lara, A., Altamirano, A., Di Bella, C., González, M.E., Julio Camarero, J., 2020. Forest browning trends in  
746 response to drought in a highly threatened mediterranean landscape of South America. Ecological Indicators 115, 106401.  
747 URL: <https://linkinghub.elsevier.com/retrieve/pii/S1470160X20303381>, doi:10.1016/j.ecolind.2020.106401.
- 748 Muñoz, A.A., Klock-Barría, K., Alvarez-Garretón, C., Aguilera-Betti, I., González-Reyes, , Lastra, J.A., Chávez, R.O.,  
749 Barría, P., Christie, D., Rojas-Badilla, M., LeQuesne, C., 2020. Water Crisis in Petorca Basin, Chile: The Combined  
750 Effects of a Mega-Drought and Water Management. Water 12, 648. URL: <https://www.mdpi.com/2073-4441/12/3/648>,  
751 doi:10.3390/w12030648.
- 752 Muñoz-Sabater, J., Dutra, E., Agustí-Panareda, A., Albergel, C., Arduini, G., Balsamo, G., Boussetta, S., Choulga, M., Harrigan,  
753 S., Hersbach, H., Martens, B., Miralles, D.G., Piles, M., Rodríguez-Fernández, N.J., Zsoter, E., Buontempo, C., Thépaut,  
754 J.N., 2021. ERA5-Land: a state-of-the-art global reanalysis dataset for land applications. Earth System Science Data 13,  
755 4349–4383. URL: <https://essd.copernicus.org/articles/13/4349/2021/>, doi:10.5194/essd-13-4349-2021.
- 756 Narasimhan, B., Srinivasan, R., 2005. Development and evaluation of Soil Moisture Deficit Index (SMDI) and Evapotranspiration  
757 Deficit Index (ETDI) for agricultural drought monitoring. Agricultural and Forest Meteorology 133, 69–88. URL: <https://linkinghub.elsevier.com/retrieve/pii/S0168192305001565>, doi:10.1016/j.agrformet.2005.07.012.
- 758 Nicolai-Shaw, N., Zscheischler, J., Hirschi, M., Gudmundsson, L., Seneviratne, S.I., 2017. A drought event composite  
759 analysis using satellite remote-sensing based soil moisture. Remote Sensing of Environment 203, 216–225. URL: <https://linkinghub.elsevier.com/retrieve/pii/S0034425717302729>, doi:10.1016/j.rse.2017.06.014.
- 760 Noguera, I., Vicente-Serrano, S.M., Domínguez-Castro, F., 2022. The Rise of Atmospheric Evaporative Demand Is Increasing

- 766 Flash Droughts in Spain During the Warm Season. *Geophysical Research Letters* 49, e2021GL097703. URL: <https://agupubs.onlinelibrary.wiley.com/doi/10.1029/2021GL097703>, doi:10.1029/2021GL097703.
- 767 Paruelo, J.M., Texeira, M., Staiano, L., Mastrángelo, M., Amdan, L., Gallego, F., 2016. An integrative index of Ecosystem  
768 Services provision based on remotely sensed data. *Ecological Indicators* 71, 145–154. URL: <https://www.sciencedirect.com/science/article/pii/S1470160X16303843>, doi:10.1016/J.ECOLIND.2016.06.054. publisher: Elsevier.
- 771 Pebesma, E., 2018. Simple Features for R: Standardized Support for Spatial Vector Data. *The R Journal* 10, 439–446. URL:  
772 <https://doi.org/10.32614/RJ-2018-009>, doi:10.32614/RJ-2018-009.
- 773 Pebesma, E., Bivand, R., 2023. *Spatial Data Science: With applications in R*. Chapman and Hall/CRC, London. URL:  
774 <https://r-spatial.org/book/>.
- 775 Peng, D., Zhang, B., Wu, C., Huete, A.R., Gonsamo, A., Lei, L., Ponce-Campos, G.E., Liu, X., Wu, Y., 2017. Country-level net  
776 primary production distribution and response to drought and land cover change. *Science of The Total Environment* 574,  
777 65–77. URL: <https://linkinghub.elsevier.com/retrieve/pii/S0048969716319507>, doi:10.1016/j.scitotenv.2016.09.033.
- 778 Pitman, A.J., De Noblet-Ducoudré, N., Avila, F.B., Alexander, L.V., Boisier, J.P., Brovkin, V., Delire, C., Cruz, F., Donat, M.G.,  
779 Gayler, V., Van Den Hurk, B., Reick, C., Volodire, A., 2012. Effects of land cover change on temperature and rainfall extremes in  
780 multi-model ensemble simulations. *Earth System Dynamics* 3, 213–231. URL: <https://esd.copernicus.org/articles/3/213/2012/>,  
781 doi:10.5194/esd-3-213-2012.
- 782 Potopová, V., Stepánek, P., Mozný, M., Türkott, L., Soukup, J., 2015. Performance of the standarised precipitation evapotranspiration index at various lags for agricultural drought risk assessment in the {C}zech {R}epublic. *Agricultural and Forest Meteorology* 202, 26–38.
- 783 R Core Team, 2023. R: A Language and Environment for Statistical Computing. R Foundation for Statistical Computing,  
784 Vienna, Austria. URL: <https://www.R-project.org/>.
- 785 Rhee, J., Im, J., Carbone, G.J., 2010. Monitoring agricultural drought for arid and humid regions using multi-sensor remote  
786 sensing data. *Remote Sensing of Environment* 114, 2875–2887. URL: <http://www.sciencedirect.com/science/article/pii/S003442571000221X>, doi:10.1016/j.rse.2010.07.005.
- 787 Rodríguez-Echeverría, J., Echeverría, C., Oyarzún, C., Morales, L., 2018. Impact of land-use change on biodiversity and ecosystem  
788 services in the Chilean temperate forests. *Landscape Ecology* 33, 439–453. URL: <http://link.springer.com/10.1007/s10980-018-0612-5>, doi:10.1007/s10980-018-0612-5.
- 789 Running, S., Zhao, M., 2019. MOD17A3HGF MODIS/Terra Net Primary Production Gap-Filled Yearly L4 Global 500 m SIN  
790 Grid V006. URL: <https://lpdaac.usgs.gov/products/mod17a3hgf006/>, doi:10.5067/MODIS/MOD17A3HGF.006.
- 791 Schulz, J.J., Cayuela, L., Echeverría, C., Salas, J., Rey Benayas, J.M., 2010. Monitoring land cover change of the dryland forest  
792 landscape of Central Chile (1975–2008). *Applied Geography* 30, 436–447. URL: <https://linkinghub.elsevier.com/retrieve/pii/S0143622809000885>, doi:10.1016/j.apgeog.2009.12.003.
- 793 Sen, P.K., 1968. Estimates of the Regression Coefficient Based on Kendall's Tau. *Journal of the American Statistical Association*  
794 63, 1379–1389. URL: <http://www.tandfonline.com/doi/abs/10.1080/01621459.1968.10480934>, doi:10.1080/01621459.1968.10480934.
- 795 Slette, I.J., Post, A.K., Awad, M., Even, T., Punzalan, A., Williams, S., Smith, M.D., Knapp, A.K., 2019. How ecologists define  
796 drought, and why we should do better. *Global Change Biology* 25, 3193–3200. URL: <https://onlinelibrary.wiley.com/doi/10.1111/gcb.14747>, doi:10.1111/gcb.14747.
- 797 Song, X.P., Hansen, M.C., Stehman, S.V., Potapov, P.V., Tyukavina, A., Vermote, E.F., Townshend, J.R., 2018. Global land  
798 change from 1982 to 2016. *Nature* 560, 639–643. URL: <https://www.nature.com/articles/s41586-018-0411-9>, doi:10.1038/s41586-018-0411-9.
- 799 Souza, A.G.S.S., Ribeiro Neto, A., Souza, L.L.D., 2021. Soil moisture-based index for agricultural drought assessment: SMADI  
800 application in Pernambuco State-Brazil. *Remote Sensing of Environment* 252, 112124. URL: <https://linkinghub.elsevier.com/retrieve/pii/S0034425720304971>, doi:10.1016/j.rse.2020.112124.
- 801 Taucare, M., Viguier, B., Figueiroa, R., Daniele, L., 2024. The alarming state of Central Chile's groundwater resources: A  
802 paradigmatic case of a lasting overexploitation. *Science of The Total Environment* 906, 167723. URL: <https://linkinghub.elsevier.com/retrieve/pii/S0048969723063507>, doi:10.1016/j.scitotenv.2023.167723.
- 803 Tennekes, M., 2018. tmap: Thematic Maps in R. *Journal of Statistical Software* 84, 1–39. doi:10.18637/jss.v084.i06.
- 804 Urrutia-Jalabert, R., González, M.E., González-Reyes, , Lara, A., Garreaud, R., 2018. Climate variability and forest fires in  
805 central and south-central Chile. *Ecosphere* 9, e02171. URL: <https://esajournals.onlinelibrary.wiley.com/doi/10.1002/ecs2.2171>,  
806 doi:10.1002/ecs2.2171.
- 807 Van Loon, A.F., Gleeson, T., Clark, J., Van Dijk, A.I., Stahl, K., Hannaford, J., Di Baldassarre, G., Teuling, A.J., Tallaksen,  
808 L.M., Uijlenhoet, R., Hannah, D.M., Sheffield, J., Svoboda, M., Verbeiren, B., Wagener, T., Rangecroft, S., Wanders, N.,  
809 Van Lanen, H.A., 2016. Drought in the Anthropocene. *Nature Geoscience* 9, 89–91. doi:10.1038/ngeo2646.
- 810 Van Loon, A.F., Van Huijgevoort, M.H.J., Van Lanen, H.A.J., 2012. Evaluation of drought propagation in an ensemble mean of  
811 large-scale hydrological models. *Hydrology and Earth System Sciences* 16, 4057–4078. URL: <https://hess.copernicus.org/articles/16/4057/2012/>, doi:10.5194/hess-16-4057-2012.
- 812 Venegas-González, A., Juñent, F.R., Gutiérrez, A.G., Filho, M.T., 2018. Recent radial growth decline in response to increased  
813 drought conditions in the northernmost Nothofagus populations from South America. *Forest Ecology and Management* 409,  
814 94–104. URL: <https://linkinghub.elsevier.com/retrieve/pii/S0378112717313993>, doi:10.1016/j.foreco.2017.11.006.
- 815 Venegas-González, A., Muñoz, A.A., Carpintero-Gibson, S., González-Reyes, A., Schneider, I., Gipolou-Zuñiga, T., Aguilera-  
816 Betti, I., Roig, F.A., 2023. Sclerophyllous Forest Tree Growth Under the Influence of a Historic Megadrought in the  
817 Mediterranean Ecoregion of Chile. *Ecosystems* 26, 344–361. URL: <https://link.springer.com/10.1007/s10021-022-00760-x>,  
818 doi:10.1007/s10021-022-00760-x.
- 819 Vicente-Serrano, S.M., Azorin-Molina, C., Sanchez-Lorenzo, A., Revuelto, J., López-Moreno, J.I., González-Hidalgo, J.C.,

- 831 Moran-Tejeda, E., Espejo, F., 2014. Reference evapotranspiration variability and trends in Spain, 1961–2011. Global  
 832 and Planetary Change 121, 26–40. URL: <https://linkinghub.elsevier.com/retrieve/pii/S0921818114001180>, doi:[10.1016/j.gloplacha.2014.06.005](https://doi.org/10.1016/j.gloplacha.2014.06.005).
- 833 Vicente-Serrano, S.M., Beguería, S., López-Moreno, J.I., 2010. A multiscale drought index sensitive to global warming: The  
 834 standardized precipitation evapotranspiration index. Journal of Climate 23, 1696–1718. URL: <http://dx.doi.org/10.1175/2009JCLI2909.1>, doi:[10.1175/2009JCLI2909.1](https://doi.org/10.1175/2009JCLI2909.1).
- 835 Vicente-Serrano, S.M., Peña-Angulo, D., Beguería, S., Domínguez-Castro, F., Tomás-Burguera, M., Noguera, I., Gimeno-Sotelo,  
 836 L., El Kenawy, A., 2022. Global drought trends and future projections. Philosophical Transactions of the Royal Society A:  
 837 Mathematical, Physical and Engineering Sciences 380, 20210285. URL: <https://royalsocietypublishing.org/doi/10.1098/rsta.2021.0285>, doi:[10.1098/rsta.2021.0285](https://doi.org/10.1098/rsta.2021.0285).
- 838 Vicente-Serrano, S.M., McVicar, T.R., Miralles, D.G., Yang, Y., Tomas-Burguera, M., 2020. Unraveling the influence of  
 839 atmospheric evaporative demand on drought and its response to climate change. WIREs Climate Change 11, e632. URL:  
 840 <https://wires.onlinelibrary.wiley.com/doi/10.1002/wcc.632>, doi:[10.1002/wcc.632](https://doi.org/10.1002/wcc.632).
- 841 Wickham, H., Averick, M., Bryan, J., Chang, W., McGowan, L.D., François, R., Grolemund, G., Hayes, A., Henry, L., Hester,  
 842 J., Kuhn, M., Pedersen, T.L., Miller, E., Bache, S.M., Müller, K., Ooms, J., Robinson, D., Seidel, D.P., Spinu, V., Takahashi,  
 843 K., Vaughan, D., Wilke, C., Woo, K., Yutani, H., 2019. Welcome to the tidyverse. Journal of Open Source Software 4, 1686.  
 844 doi:[10.21105/joss.01686](https://doi.org/10.21105/joss.01686).
- 845 Wilhite, D.A., Glantz, M.H., 1985. Understanding: The drought phenomenon: The role of definitions. Water International 10,  
 846 111–120. URL: <http://dx.doi.org/10.1080/02508068508686328>, doi:[10.1080/02508068508686328](https://doi.org/10.1080/02508068508686328).
- 847 Wilks, D.S., 2011. Empirical distributions and exploratory data analysis. Statistical Methods in the Atmospheric Sciences 100.
- 848 Winkler, K., Fuchs, R., Rounsevell, M., Herold, M., 2021. Global land use changes are four times greater than previously estimated.  
 849 Nature Communications 12, 2501. URL: <https://www.nature.com/articles/s41467-021-22702-2>, doi:[10.1038/s41467-021-22702-2](https://doi.org/10.1038/s41467-021-22702-2).
- 850 WMO, Svoboda, M., Hayes, M., Wood, D.A., 2012. Standardized Precipitation Index User Guide. WMO, Geneva. URL:  
 851 [http://library.wmo.int/opac/index.php?lvl=notice\\_display&id=13682](http://library.wmo.int/opac/index.php?lvl=notice_display&id=13682). series Title: WMO Publication Title: WMO-No. 1090  
 852 © Issue: 1090.
- 853 Wright, M.N., Ziegler, A., 2017. ranger: A Fast Implementation of Random Forests for High Dimensional Data in C++ and R.  
 854 Journal of Statistical Software 77, 1–17. doi:[10.18637/jss.v077.i01](https://doi.org/10.18637/jss.v077.i01).
- 855 Wu, C., Zhong, L., Yeh, P.J.F., Gong, Z., Lv, W., Chen, B., Zhou, J., Li, J., Wang, S., 2024. An evaluation framework for  
 856 quantifying vegetation loss and recovery in response to meteorological drought based on SPEI and NDVI. Science of The  
 857 Total Environment 906, 167632. URL: <https://linkinghub.elsevier.com/retrieve/pii/S0048969723062599>, doi:[10.1016/j.scitotenv.2023.167632](https://doi.org/10.1016/j.scitotenv.2023.167632).
- 858 Xiao, C., Zaehle, S., Yang, H., Wigneron, J.P., Schmullius, C., Bastos, A., 2023. Land cover and management effects on ecosystem  
 859 resistance to drought stress. Earth System Dynamics 14, 1211–1237. URL: <https://esd.copernicus.org/articles/14/1211/2023/>,  
 860 doi:[10.5194/esd-14-1211-2023](https://doi.org/10.5194/esd-14-1211-2023).
- 861 Yang, J., Huang, X., 2021. The 30 m annual land cover dataset and its dynamics in China from 1990 to 2019. Earth System  
 862 Science Data 13, 3907–3925. URL: <https://essd.copernicus.org/articles/13/3907/2021/>, doi:[10.5194/essd-13-3907-2021](https://doi.org/10.5194/essd-13-3907-2021).
- 863 Zambrano, F., 2023a. Data of monthly climate variables and drought indices within continental Chile for 1981–2023. URL:  
 864 <https://zenodo.org/doi/10.5281/zenodo.10359546>, doi:[10.5281/ZENODO.10359546](https://doi.org/10.5281/ZENODO.10359546).
- 865 Zambrano, F., 2023b. Four decades of satellite data for agricultural drought monitoring throughout the growing season in  
 866 Central Chile, in: Vijay P. Singh Deepak Jhajharia, R.M., Kumar, R. (Eds.), Integrated Drought Management, Two Volume  
 867 Set. CRC Press, p. 28.
- 868 Zambrano, F., Lillo-Saavedra, M., Verbist, K., Lagos, O., 2016. Sixteen years of agricultural drought assessment of the  
 869 biobío region in chile using a 250 m resolution vegetation condition index (VCI). Remote Sensing 8, 1–20. URL: <http://www.mdpi.com/2072-4292/8/6/530>, doi:[10.3390/rs8060530](https://doi.org/10.3390/rs8060530). publisher: Multidisciplinary Digital Publishing Institute.
- 870 Zambrano, F., Vrielinck, A., Nelson, A., Meroni, M., Tadesse, T., 2018. Prediction of drought-induced reduction of agricultural  
 871 productivity in Chile from MODIS, rainfall estimates, and climate oscillation indices. Remote Sensing of Environment  
 872 219, 15–30. URL: <https://www.sciencedirect.com/science/article/pii/S0034425718304541>, doi:[10.1016/j.rse.2018.10.006](https://doi.org/10.1016/j.rse.2018.10.006).  
 873 publisher: Elsevier.
- 874 Zhao, Y., Feng, D., Yu, L., Wang, X., Chen, Y., Bai, Y., Hernández, H.J., Galleguillos, M., Estades, C., Biging, G.S., Radke,  
 875 J.D., Gong, P., 2016. Detailed dynamic land cover mapping of Chile: Accuracy improvement by integrating multi-temporal  
 876 data. Remote Sensing of Environment 183, 170–185. URL: <https://linkinghub.elsevier.com/retrieve/pii/S0034425716302188>,  
 877 doi:[10.1016/j.rse.2016.05.016](https://doi.org/10.1016/j.rse.2016.05.016).
- 878 Zhou, K., Li, J., Zhang, T., Kang, A., 2021. The use of combined soil moisture data to characterize agricultural drought  
 879 conditions and the relationship among different drought types in China. Agricultural Water Management 243, 106479. URL:  
 880 <https://linkinghub.elsevier.com/retrieve/pii/S0378377420305965>, doi:[10.1016/j.agwat.2020.106479](https://doi.org/10.1016/j.agwat.2020.106479).